IEEE Access
Multidisciplinary | Rapid Review | Open Access Journal

Received June 17, 2020, accepted July 10, 2020, date of publication July 16, 2020, date of current version July 29, 2020.

Digital Object Identifier 10.1109/ACCESS.2020.3009850

A Pragmatic Approach to Massive MIMO for Broadband Communication Satellites

PIERO ANGELETTI, (Senior Member, IEEE), AND RICCARDO DE GAUDENZI, (Senior Member, IEEE)
European Space Agency, 2200 AG Noordwijk, The Netherlands
Corresponding author: Riccardo De Gaudenzi (rdegaude@gmail.com)

ABSTRACT In this paper, we analyze the performance of Massive Multiple Input Multiple Output (M-MIMO) techniques aiming at increasing the throughput of broadband satellites. In particular, we investigate a ''pragmatic'' approach to the design of the M-MIMO to ease its implementation both at system and satellite payload level. We compare the performance of optimized classical Minimum Mean Square Error (MMSE), Zero Forcing (ZF), Matched Filter (MF) schemes with the proposed ''pragmatic'' M-MIMO one dubbed fixed Multi-Beam (MB). To further boost the M-MIMO performance, a novel radio resource management approach based on Mixed Integer Quadratic Programming (MIQDP-RRM) is proposed. The adoption of MIQDP-RRM is shown to greatly enhance the M-MIMO throughput performance. It is shown that the MB scheme closely approximate the MF, ZF and MMSE performance with a much simpler active antenna-based payload architecture and without requiring any user channel estimation. The MB MIQDP–RRM M-MIMO pragmatic solution allows to achieve higher satellite broadband throughput compared to a conventional four colors frequency reuse scheme (CFR) with affordable complexity for both space and ground segments. At the same time we show that by non-conventional CFR multi-beam array design, the performance gap compared to MB MIQDP–RRM M-MIMO can be significantly reduced.

INDEX TERMS MIMO, satellite communications, antenna arrays, multiplexing, payloads.

I. INTRODUCTION AND MOTIVATION

Recent years have witnessed a strong impulse in adopting Massive Multiple input Multiple Output (M-MIMO) in wireless networks [1], [2]. Despite the wide literature related to M-MIMO for terrestrial networks, much less attention has been devoted to its possible exploitation in the forward link of satellite systems. So far the satellite communication research has been largely focused on the applicability of MIMO precoding techniques to current satellite payloads characterized by single feed per beam architecture. In particular, satellite specific issues like multicasting, multiple gateways, channel estimation have been reported in the literature [3]–[8]. The fact that current satellite forward link standards like DVB-S2X [9], are requiring to multiplex packets belonging to different users in the same physical layer frame, has an important impact on precoding performance due to this ''multicasting'' effect. Techniques to partially mitigate this problem, based on multiplexing on the same physical layer frame packets with similar channel characteristics have been devised in [5].

The associate editor coordinating the review of this manuscript and approving it for publication was Davide Ramaccia.

Another issue is related to the fact that high throughput broadband satellite networks needs a large number of user beams which are mapped in the feeder link on a number of spatially separated gateways [8]. Due to satellite payload complexity limitations, the precoding is assumed to be implemented at the gateway. Consequently, each gateway will only be able to precode the assigned subset of user's beams. Thus precoding from separated gateways results to be less effective in mitigating co-channel interference. Centralized precoding with interconnected gateways was proposed as a possible solution to this problem, but resulted to be not very cost effective because of the high rate terrestrial gateway interconnection links required. The issue of limited number of beams precoded by each gateway can be alleviated by combining precoding and beam hopping [10]. Another satellite specific effect is related to the delay in channel reports due to the intrinsic propagation delay which is particularly large in geostationary satellite. However, this effect was found in [7] to have a negligible performance impact. The precoding requires keeping the satellite payload beam chains controlled in relative phase and amplitude. This makes the payload implementation more complex compared to

conventional systems [7]. Furthermore, for satellites in non geostationary orbit (e.g. mega-constellations) the fast orbit dynamic makes the adoption of conventional precoding techniques even more challenging.

The possible advantages of combining precoding with beamforming were investigated in [11]. Despite the increased degrees of freedom, this approach showed limited performance advantage. In defiance to these not very encouraging findings, the recent momentum in developing flexible multibeam payloads based on active antennas is opening up new opportunities for exploiting M-MIMO in satellite communications [12]. The objective of the current paper is to investigate the potential advantages and, even more important, to devise practical ways to implement solution approaching the M-MIMO performance. The key challenges we are facing for adopting M-MIMO in broadband satellite networks can be summarized as:

1) Difficulties in the practical implementation of M-MIMO technology because:
   a) Wide adoption of transparent payloads with distributed gateways and four colors frequency reuse schemes not compatible with M-MIMO.
   b) Very limited adoption of active array antennas with a large number of radiating elements.
   c) Impossibility to use Time Division Duplexing (TDD) schemes to ease channel estimation because of satellite frequency regulation restrictions in millimeter wave bands.
   d) Cumbersome implementation of pre-coding schemes requiring user feedback in satellite Frequency Division Duplexing (FDD) scheme.
   e) Limitations in the amount digital processing implementable on-board.
2) Benign channel model, essentially Additive White Gaussian Noise (AWGN) with no multipath fading, reducing the potential M-MIMO performance gain.

Points 1-a) and 1-b) are mainly related to the legacy systems design and technological issues implementing active antennas at millimeter frequency bands. However, these issues are currently being tackled by industry R&D with expected large spin-in from terrestrial wireless technologies being developed for the 5G New Radio at millimeter bands [13]. Point 1-c) is particularly critical as TDD can not be used in the Ku/Ka/Q-band satellite bands commonly adopted by broadband systems. Point 1-d) is related to the difficulty in performing FDD channel estimation with FDD as well as the non scalability of M-MIMO pilot-based channel estimation [1]. As a consequence, the FDD scheme adopted in these bands is not compatible with M-MIMO unless for very small scale systems of no practical interest. Point 1-e) is related to the on-board processor power consumption, heat dissipation and mass constraints limiting the M-MIMO digital signal processing possible even on a high throughput satellite. While the implementation of adaptive wide-band digital beam forming is considered very challenging, on-board implementation of algorithms requiring matrix inversions is considered to be out of scope even in the medium term. Moving the M-MIMO signal processing to the gateway will require a very large increase of the feeder link bandwidth as well the previously mentioned need for high-speed gateways' interconnection.

Point 2 was also considered a major drawback of broadband satellite systems operating in AWGN channel. In fact one of the M-MIMO advantages is to "transform" uncorrelated (Rayleigh) fading channels into an AWGN one (the so called channel hardening [1]). This property can not be exploited in satellite broadband M-MIMO systems. However, following [14] this issue may be circumvented by proper system design.

In a nutshell, the main objectives of the manuscript are: a) To properly model M-MIMO for broadband satellite networks; b) To derive an adequate, yet feasible, Radio Resource Management (RRM) strategy; c) To identify affordable complexity payload/system solutions allowing practical M-MIMO implementation with acceptable performance losses; d) To understand the potential performances of M-MIMO for broadband satellite networks and to compare them with more conventional approaches.

The rest of the paper is organized as follows: Sec. II describes the satellite M-MIMO system model. Sec. III summarizes the performance results of the various M-MIMO solutions investigated. Sec. IV contains the results for conventional frequency reuse scheme. Sec. V provides a summary of the results corresponding to the optimized configurations. Sec. VI describes a pragmatic payload design achieving performance close to the ideal M-MIMO with affordable complexity. Finally Sec. VII provides the summary and conclusions.

II. SYSTEM MODEL

To analyze the performance of the various M-MIMO schemes and to compare them with more conventional payload architecture we have been developing an overall system model encompassing both the space and the user segments. To ease the results comparison and to focus on the key sizing parameters the following approximations have been made: 1) Global antenna coverage of the Earth above a minimum elevation angle; 2) Linear payload characteristic; 3) Negligible feeder uplink AWGN effect; 4) Ideal channel estimation for precoding. A high-level representation of the forward-link payload and satellite-user geometry is represented in Fig. 1. The left inputs are corresponding to the N_U user beam inputs entering the On-Board Processor (OBP). These N_U signals are coming from the gateways feeder uplink and down-converted to a frequency compatible with the OBP. The OBP implements N_U distinct beam-forming networks, one for each beam input. Each Beam Forming Network (BFN) has N_T outputs (one for each antenna feed). For each of the N_T Radio Frequency (RF) feed chains, the N_U BFN outputs are summed together before being converted to the user downlink frequency and amplified. The antenna radiates towards the satellite coverage region (or Region of

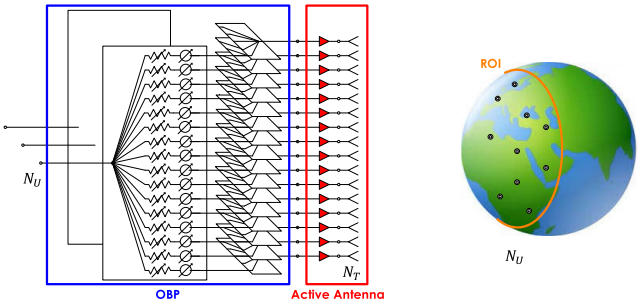

FIGURE 1. Sketch representation of the forward-link payload and satellite-user geometry.

Interest - ROI) the N_T feed signals simultaneously. Each antenna feed element contains a linear combination, properly weighted in amplitude and phase, of the N_U beam signals. The circular ROI as per point 1) simplifies the analysis while maintaining full generality. Arbitrary coverage patterns within this circular boundary are possible thanks to the payload resource allocation flexibility. The High Power Amplifiers (HPAs) present in the Direct Radiating Array (DRA) on-board antenna will operate in multi-carrier mode, thus they will require to operate at a certain back-off from the amplifier compression point. Consequently, as for point 2), we considered the HPAs as linear devices. Intermodulation effects, although mitigated by the DRA payload architecture [15], can be accounted as additional AWGN. Finally, the feeder uplink is typically designed to make its noise contribution to the overall forward link negligible. Hence, the assumption 3) is well justified. Assumption 4) is clearly optimistic, although no satellite specific M-MIMO analysis of this effect can be found in open literature. While for single feed per beam satellite payloads, pre-coding channel state information (CSI) errors impact has been estimated [7], such results is not-available for a M-MIMO DRA architecture. In particular, the CSI phase errors will have a direct impact on the beam shape which was not the case for the single-feed per beam precoding discussed in literature. Anyway, as we are interested in assessing pragmatic M-MIMO solutions not requiring per user CSI, in the following we will consider ideal CSI pre-coding as the M-MIMO performance upper bound.

To simulate the random traffic distribution, we implemented a Monte Carlo approach. At each iteration we randomly generate the N_U simultaneous users' location over the satellite coverage region. More than N_U[1] users, can be supported exploiting Time Division Multiplexing (TDM) as typically implemented in satellite broadband systems. At each iteration step the system performance (see Sec. II-E) are computed. The process is repeated N_{iter} times to accumulate a sufficient number of independent statistics to properly characterize the system behavior.

[1]The parameter N_T/N_U where N_T represents the number of the Direct Radiating Antenna (DRA) elements, will be optimized by simulation to maximize the system throughput.

A. PAYLOAD, ANTENNA AND CHANNEL MODEL

To simplify the notation and system analysis we initially focus on a payload sub-band occupied by a single time division multiplexed (TDM) carrier. The extension to a payload using multiple sub-bands and carriers in a combined Frequency Division Multiplexing (FDM) and TDM fashion is straightforward. We assume an ideal payload composed of an on-board processor implementing the digital beamforming or pre-coding matrix which maps the N_U active users per TDM carrier to the N_T antenna radiating elements as shown in Fig. 1.

We will use the following notation: vectors will be represented in bold lower-case and matrices in bold capital letters; bold italics will be used for vectors and matrices representing geometrical positions (in the real and Fourier space). Superscripts T and H will indicate transpose and complex conjugate transpose matrix operators, respectively.

The input signals, the transmitted signals and the received signals can be collected in the column vectors $\mathbf{x} = [x_1, \ldots, x_j, \ldots, x_{N_U}]^T$, $\mathbf{y} = [y_1, \ldots, y_n, \ldots, y_{N_T}]^T$ and $\mathbf{z} = [z_1, \ldots, z_i, \ldots, z_{N_U}]^T$, where x_j, y_n and z_i are the complex input signal for user j, the complex signals transmitted by radiating element n and the complex signal received by receiver i, respectively. The transfer function between the input ports of the N_T antenna radiating elements and the N_U user receiver outputs can be described by a complex channel matrix $\mathbf{H}$ of dimensions $[N_U \times N_T]$ where the generic entry element $h_{i,n}$ describes the complex transfer function between the input of the transmit radiating element n and the input of the user i receiver. Similarly, the relationship between signals at the input ports and the signals at the output ports of the precoding/beamforming OBP can be expressed by means of a complex transfer matrix $\mathbf{U}$ of dimensions $(N_T \times N_U)$ where the generic matrix element $u_{n,j}$ describe the complex transfer function between the input port j and output port n.

For simplicity, as mentioned before, it is assumed that all the antenna power amplifiers are identical and do not introduce amplitude and phase errors so that their effect can be absorbed in a single scaling constant proportional to the overall RF payload power P_T. Relevant normalization of the precoding/beamforming matrix, $\hat{\mathbf{U}}$, is discussed in Sec. II-D. The resulting signal flow graph is shown in Fig. 2. The input-output representation is summarised by the equation

$$\mathbf{y} = \sqrt{P_T}\hat{\mathbf{U}}\mathbf{x}, \quad \mathbf{z} = \mathbf{H}\mathbf{y} + \mathbf{n} = \sqrt{P_T}\mathbf{H}\hat{\mathbf{U}}\mathbf{x} + \mathbf{n}, \qquad (1)$$

where $\mathbf{n}$ is a vector whose elements represents the random noise process (thermal plus possible external inter-system interference) experienced by the N_U user.

Without loss of generality we can assume that all the users have identical terminals and experience same receive noise power. Scaling (1) such that the noise random variables have unitary variance, we can represent the noise signal vector $\mathbf{n}$ as Independent and Identically Distributed (IID) random variables with a circularly-symmetric complex Gaussian distribution of zero mean and unitary variance (the absorption

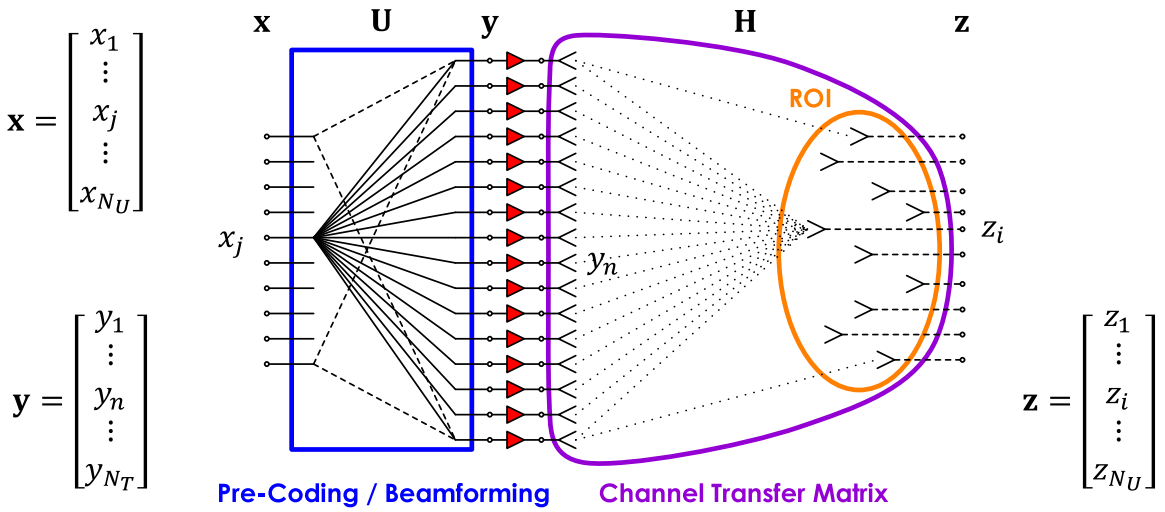

FIGURE 2. Signal flow graph.

of the noise standard deviation as scaling factor of the the channel matrix is described in Sec. II-B4).

B. CHANNEL MATRIX

The channel matrix $\mathbf{H}$ represents the complex transfer function between each radiating element of the on-board antenna array and the user receivers. At each iteration, a distribution of users is generated over the region of interest defined by a minimum satellite elevation angle on Earth, which corresponds to a circle in the satellite $[u, v]$ coordinates. The satellite-Earth geometry and relevant coordinate systems are depicted in Fig. 3 and they satisfy the following relationships

$$u_i = \sin(\vartheta_i)\cos(\phi_i), \quad v_i = \sin(\vartheta_i)\sin(\phi_i),$$
$$\vartheta_i = \sqrt{u_i^2 + v_i^2}, \quad \phi_i = \tan^{-1}\left(\frac{v_i}{u_i}\right). \tag{2}$$

Two different spatial distribution statistics have been implemented and are shortly described hereafter.

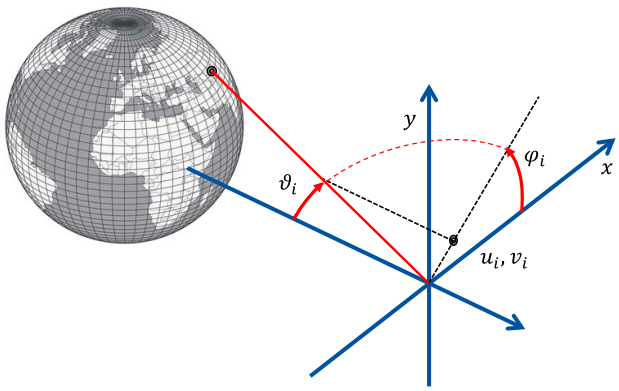

FIGURE 3. Satellite-Earth geometry and relevant coordinate systems.

1) UNIFORM SPATIAL DISTRIBUTION IN A CIRCLE

The user distribution consists of N_U realizations of two independent random variables $[\zeta_1, \zeta_2]$ each of them uniformly distributed in $[0, 1]$ and mapped in the u, v disk of radius $\sin(\vartheta_{\max})$ by means of inverse transform sampling.

$$\begin{aligned}\rho_i &= \sin(\vartheta_{\max})\sqrt{\zeta_1}\\ \phi_i &= 2\pi\ \zeta_2\\ \vartheta_i &= \sin^{-1}(\rho_i)\end{aligned} \qquad \boldsymbol{u}_i = \begin{bmatrix} u_i \\ v_i \end{bmatrix} = \begin{bmatrix} \rho_i\cos(\phi_i) \\ \rho_i\sin(\phi_i) \end{bmatrix}. \tag{3}$$

2) POISSON DISK DISTRIBUTION IN A CIRCLE

In addition to uniformity within the circle defining the region of interests, the N_U realizations must satisfy the constraint that each point is separated from the others by a minimum distance 2ρ, where the parameter $\rho_{\min}$ is called the Poisson disk radius. The advantage of the minimum distance distribution for M-MIMO will be apparent in Sec. III. Several algorithms have been proposed for Poisson disk sampling [16]. In our implementation we start from a uniform point distribution which is evolved in an iterative fashion to finally satisfy the minimum distance requirements to be representative of the RRM approach described in Sec. II-G. The evolution is performed according to molecular dynamics principles with a repulsive force repelling points closer than the Poisson disk radius. The difference between the two spatial distribution can be appreciated in Fig. 4 and Fig. 5 where 100 points are generated uniformly and according to a Poisson disk distribution with minimum separation of 0.5 degrees (i.e. Poisson disk radius of 0.25 degrees), respectively. The way to practically achieve this minimum distance distribution starting from an uniform users' distribution applying a specific RRM solution is described in Sec. II-G.

3) ACTIVE ANTENNA CHANNEL MODEL

The on-board active antenna is modelled as a square planar array of size $D_A \times D_A$ composed of N_T radiating elements

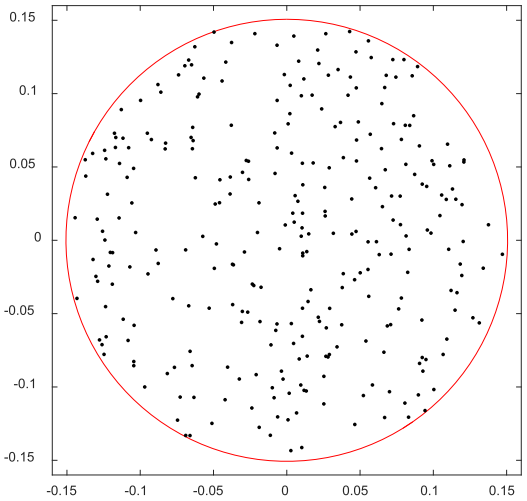

FIGURE 4. Uniform user distribution.

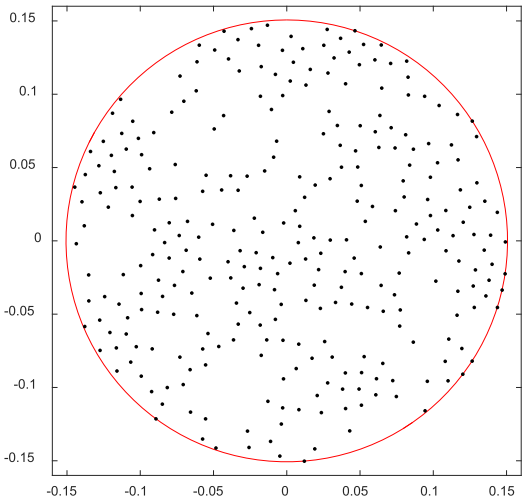

FIGURE 5. Poisson disk user distribution.

placed on a square lattice with element spacing d_A. Let $\boldsymbol{r}_n$ denote the position of the n-th array element, $g_n(\vartheta, \phi)$ the co-polar radiation pattern referred to the common antenna coordinate origin and w_n the complex array excitation coefficients. The total co-polar radiation pattern can be written as

$$g(\vartheta, \phi) = \sum_{n=1}^{N_T} w_n g_n(\vartheta, \phi) = \mathbf{g}(\vartheta, \phi)\mathbf{w}, \tag{4}$$

where $\mathbf{w} = [w_1, \ldots, w_n, \ldots, w_{N_T}]^T$ is the column vector of the array complex weights normalised to unit norm, $||\mathbf{w}||^2 = \sum_{n=1}^{N_T} w_n^2 = 1$, and $\mathbf{g}(\vartheta, \phi) = [g_1(\vartheta, \phi), \ldots, g_n(\vartheta, \phi), \ldots, g_{N_T}(\vartheta, \phi)]$ is the array manifold row vector which incorporate all the spatial characteristics of the far-field radiation patterns of the array elements. Assuming that all the radiating elements are identical and equally oriented in space with a common element radiation pattern $g_E(\vartheta, \phi)$, we can use the far-field approximation [17] to express the radiation pattern of the n-th element $g_n(\vartheta, \phi)$ with phase center corresponding to the position $\boldsymbol{r}_n = x_n\hat{\boldsymbol{x}} + y_n\hat{\boldsymbol{y}}$, where $\hat{\boldsymbol{x}}$ and $\hat{\boldsymbol{y}}$ are the coordinate direction unit vectors, thus

$$g_n(\vartheta, \phi) = g_E(\vartheta, \phi) \cdot \exp[jk_0(x_n \sin\vartheta \cos\phi + y_n \sin\vartheta \sin\phi)], \tag{5}$$

being $k_0 = 2\pi/\lambda$ the free-space wave-number, $\lambda = f_0/c$ the free-space wavelength, f_0 the carrier frequency and c the speed of light. Concerning the element radiation pattern $g_E(\vartheta, \phi)$, the simple rotationally symmetric model discussed in [18] has been used with $g_E(\vartheta, \phi) = g_E(\vartheta)$ defined as

$$g_E(\vartheta) = \sqrt{G_E^{\max}} \cos^{q_E}(\vartheta), \qquad \begin{aligned} G_E^{\max} &= 4\pi A_E 10^{\frac{\eta_E(\mathrm{dB})}{10}}, \\ q_E &= \tfrac{1}{4} G_E^{\max} - \tfrac{1}{2}, \end{aligned} \tag{6}$$

where $G_E^{\max}$ is the peak gain of the radiating element and A_E is the DRA elementary cell area normalised to the wavelength squared, $A_E = (d_A/\lambda)^2$ and $\eta_E(\mathrm{dB})$ is the radiating element efficiency expressed in dB. It is worth noting that efficiency affects the exponent and in turn the gain, so it should be considered an aperture efficiency.

4) LINK BUDGET MODEL

The path from the satellite active array to the i-th user can be described by a "normalized" link budget parameter $L_{\mathrm{B}}(\vartheta_i)$ defined as the signal gain from the satellite array center of coordinates to the user receiver antenna output over the noise power. In the following, for notation simplicity, we assume that the receiver noise temperature is independent from the atmospheric attenuation. The more general formulation for the user terminal noise temperature dependency on the atmospheric attenuation can be found in [19] and [20]. We also neglect the effect of atmospheric fading which has been shown to have negligible impact on the average system throughput [19]. With the above simplifications at hand, the $L_{\mathrm{B}}(\vartheta_i)$ coefficient can be computed as

$$\begin{aligned} L_B(\vartheta_i) &= \frac{G_R^U}{L_{FS}(\vartheta_i) N_R^U}, \quad L_{FS}(\vartheta_i) = \left[\frac{4\pi r(\vartheta_i)}{\lambda}\right]^2, \\ r(\vartheta_i) &= \Big[(R_E + H_S)^2 + R_E^2 - 2R_E(R_E + H_S)\sin(\alpha_i) \\ &\quad + \sin^{-1}\left(\frac{R_E}{R_E + H_S}\right)\cos(\alpha_i)\Big]^{\frac{1}{2}}, \\ \alpha_i &= \cos^{-1}\left[\sin(\vartheta_i)\frac{(R_E + H_S)}{R_E}\right], \quad N_R^U = K_B T_R^U R_s, \end{aligned} \tag{7}$$

where G_R^U is the receive user terminal antenna gain, T_R^U is the user antenna temperature, K_B is the Boltzmann constant, R_E is the Earth radius, H_S is the satellite orbit altitude, ϑ_i and α_i are the off-nadir satellite angle and the over the horizon elevation angle, respectively, for the i-th user with $0 \le \vartheta_i \le \vartheta_{\max}$ being $\vartheta_{\max}$ derived as

$$\vartheta_{\max}(\alpha_{\min}) = \sin^{-1}\left(\frac{R_E}{R_E + H_S}\right)\cos(\alpha_{\min}), \tag{8}$$

where $\alpha_{\min}$ is the minimum allowed satellite elevation angle. The ROI's surface, dubbed A_c, can be computed as

$$A_c(\alpha_{\min}) = 2\pi R_E^2 \cos\left[\frac{\pi}{2} - \vartheta_{\max}(\alpha_{\min}) - \alpha_{\min}\right]. \quad (9)$$

5) CHANNEL MATRIX DECOMPOSITION

Observing that the normalised link budget parameter $L_B(\vartheta_i)$ (7) and the elementary radiation pattern $g_E(\vartheta_i)$ (6) depend only on the user index i, and that the phase of the n-th element pattern (5) depends on both the indexes i and n, we can decompose the channel matrix $\mathbf{H}$ as the element-wise product of an amplitude matrix $\mathbf{H}_{\text{AMP}}$ and a phase matrix $\mathbf{H}_{\text{PH}}$, both of size $(N_U \times N_T)$ as $\mathbf{H} = \mathbf{H}_{\text{AMP}} \odot \mathbf{H}_{\text{PH}}$, where $\odot$ indicates the Hadamard product and

$$\mathbf{H}_{\text{AMP}} = \begin{bmatrix} h_{\text{AMP}}(1) & \cdots & h_{\text{AMP}}(1) \\ \vdots & & \vdots \\ h_{\text{AMP}}(N_U) & \cdots & h_{\text{AMP}}(N_U) \end{bmatrix}, \quad (10)$$

$$\mathbf{H}_{\text{PH}} = \begin{bmatrix} h_{\text{PH}}(1,1) & \cdots & h_{\text{PH}}(1,N_T) \\ \vdots & & \vdots \\ h_{\text{PH}}(N_U,1) & \cdots & h_{\text{PH}}(N_U,N_T) \end{bmatrix}, \quad (11)$$

with

$$h_{\text{AMP}}(i) = g_E(\vartheta_i) L_B(\vartheta_i) \quad (12)$$

$$h_{\text{PH}}(n,i) = \exp\left[jk_0(x_n \sin\vartheta_i \cos\phi_i + y_n \sin\vartheta_i \sin\phi_i)\right]. \quad (13)$$

Recalling (2), then (13) can be rewritten as

$$h_{\text{PH}}(n,i) = \exp\left[jk_0(x_n u_i + y_n v_i)\right] = \exp\left(jk_0\, \boldsymbol{r}_n \cdot \boldsymbol{u}_i\right), \quad (14)$$

where the operator $\cdot$ represents the scalar product between vectors.

C. PRECODING AND BEAMFORMING MATRICES

The complex matrix $\mathbf{U}$ represents the generic $(N_T \times N_U)$ precoding/beamforming matrix described as

$$\mathbf{U} = \begin{bmatrix} u(1,1) & \cdots & u(1,N_U) \\ \vdots & & \vdots \\ u(N_T,1) & \cdots & u(N_T,N_U) \end{bmatrix}. \quad (15)$$

The j-th column vector of $\mathbf{U}$ represents the array beamforming complex weights for the j-th user

$$\mathbf{u}_j^{\text{C}} = \begin{bmatrix} u(1,j) \\ \vdots \\ u(N_T,j) \end{bmatrix}. \quad (16)$$

The beamforming weight vector $\mathbf{u}_j^{\text{C}}$, normalised to unit magnitude $\mathbf{w}_j = \mathbf{u}_j^{\text{C}}/||\mathbf{u}_j^{\text{C}}||$, determines the "shape" of the relevant radiation pattern, $\mathbf{g}(\vartheta,\phi)\mathbf{w}_j$, for the j-th input.

The overall matrix $\mathbf{U}$ can be decomposed in a set of column vectors

$$\mathbf{U} = \begin{bmatrix} \mathbf{u}_1^{\text{C}} & \cdots & \mathbf{u}_{N_U}^{\text{C}} \end{bmatrix}. \quad (17)$$

In the following, we will identify the various M-MIMO techniques by the $\mathbf{U}$ subscript.

1) MATCHED FILTER

The basic principle of the Matched Filter[2] (MF) is derived from diversity combining techniques [21] and correspond to maximization of the realized gain of the array [22] obtained as

$$\mathbf{U}_{\text{MF}} = \mathbf{H}^H. \quad (18)$$

It can be observed that for a direct radiating array the i-th row of the phase matrix (11) corresponds to the array response vector in the i-th user direction. The transpose conjugate operation can be interpreted as the generation of a steering vector such that the corresponding array factor is pointed to the i-th user direction.

2) SWITCHABLE FIXED MULTI-BEAM

Bearing in mind the observation about the correspondence of the MF to a beam steering, an approximation of the beamforming vectors can be based on the selection from a pre-defined set of the steering vector with the nearest bore-sight to the user direction. Different criteria can be used to define the set of beam positions uniquely determining the pre-defined steering vectors (e.g. uniform or non-uniform distribution). In the following, we describe a regular sampling of the zone of interest based on a lattice of beam positions. As shown in Sec. VI, this approach has important implementation complexity advantages. The bi-dimensional lattice of beam positions can be defined in terms of basis vectors $\boldsymbol{s}_1$ and $\boldsymbol{s}_2$ and basis matrix $\boldsymbol{S}$:

$$\boldsymbol{s}_1 = \begin{bmatrix} s_{1u} \\ s_{1v} \end{bmatrix}, \quad \boldsymbol{s}_2 = \begin{bmatrix} s_{2u} \\ s_{2v} \end{bmatrix}, \quad \boldsymbol{S} = \left[\boldsymbol{s}_1, \boldsymbol{s}_2\right]. \quad (19)$$

Any point of the lattice can be represented as a superposition of integer multiples of the basis vectors $\boldsymbol{s}_1$ and $\boldsymbol{s}_2$. The column vectors $\boldsymbol{s}_1$ and $\boldsymbol{s}_2$ are linearly independent and the matrix $\boldsymbol{S}$ non-singular. The set of all linear combinations of $\boldsymbol{s}_1$ and $\boldsymbol{s}_2$ with integer coefficients defines the bi-dimensional lattice $\Lambda(\boldsymbol{S})$ [23]. Considering that the main beam gain will decay proportionally to the squared distance from be beam center, the assignment of far field points in the region of interest to the beam with maximum gain will correspond to a Voronoi tessellation of the u, v plane. The concepts of the regular lattice and associated Voronoi tessellation are illustrated in Fig 6. Considering that an hexagonal packing of beams offers optimal cross-over performance and reduction of number of beams for a target cross-over level, the lattice of beam centers can be generated by an hexagonal lattice base matrix $\boldsymbol{S}_{\text{MB}}$ with beam-to-beam inter-distance controlled by a normalised beam spacing S_{MB}^n referred to the array normalised angular beam-width[3] λ/D_{A} derived

[2] In M-MIMO literature often the term Maximal Ratio (MR) combining is used instead of MF.

[3] λ/D_A corresponds, for a uniformly excited linear array of size D_{A}, to the first null position and to about 4dB beam-width, both in u space.

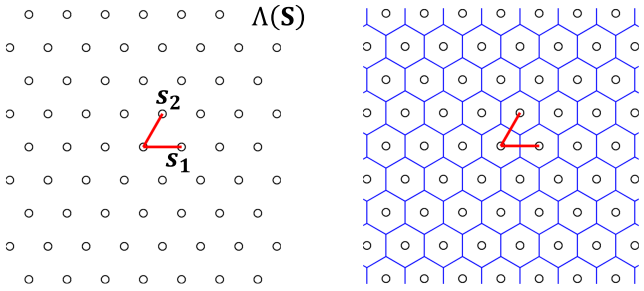

FIGURE 6. Beam lattice geometry and Voronoi tessellation.

as

$$\boldsymbol{S}_{\mathrm{MB}} = S^{n}_{\mathrm{MB}} \frac{\lambda}{D_A} \begin{bmatrix} 1 & \frac{1}{2} \\ 0 & \frac{\sqrt{3}}{2} \end{bmatrix}. \tag{20}$$

The pre-defined set of beams centers $\boldsymbol{s}_k$ can be evaluated as the intersection of lattice of points $\Lambda(\boldsymbol{S}_{\mathrm{MB}})$ and the u, v disk of radius $\sin[\vartheta_{\max}(\alpha_{\min})]$ as

$$\{\boldsymbol{s}_k\} = \Lambda(\boldsymbol{S}_{\mathrm{MB}}) \cap \{|\boldsymbol{u}| \leq \sin[\vartheta_{\max}(\alpha_{\min})]\}. \tag{21}$$

The set of pre-defined beam centers $\{\boldsymbol{s}_k\}$ plays the role of a code-book in a vector quantization of the u, v region of interest. The bi-dimensional quantizer is defined by the Voronoi partition of the space into non overlapping cells. A user position vector $\boldsymbol{u}_i$ is encoded comparing it with the set of pre-defined beam centers which act as code vectors. A user is assigned to the beam with closest beam center. We shortly indicate the assignment of $\boldsymbol{u}_i$ to $\boldsymbol{s}_k$ as the quantization BEAM(i) derived as

$$\mathrm{BEAM}(i) = \underset{k}{\operatorname{argmin}} \|\boldsymbol{s}_k - \boldsymbol{u}_i\|^2. \tag{22}$$

Although, as it will be discussed in Sec. VI, the process of performing the beam quantization and generation of the associated steering vector is better realised through the cascade of a beam selection matrix and fixed beamforming network or some hybrid beamforming structure, the resulting precoding/beamforming matrix is described by the phase matrix

$$\mathbf{U}_{\mathrm{MB}} = \begin{bmatrix} u_{\mathrm{MB}}(1,1) & \cdots & u_{\mathrm{MB}}(1,N_U) \\ \vdots & & \vdots \\ u_{\mathrm{MB}}(N_T,1) & \cdots & u_{\mathrm{MB}}(N_T,N_U) \end{bmatrix}, \tag{23}$$

where the generic (n, j) entry element is $u_{\mathrm{MB}}(n,j) = \exp\left(-jk_0\, \boldsymbol{r}_n \cdot \boldsymbol{s}_{\mathrm{BEAM}(j)}\right)$.

3) ZERO FORCING

The Zero Forcing (ZF) precoding approach corresponds to the search of the optimum transmit vector $\hat{\mathbf{y}}$ at the output of the array which, once received by the users through the channel matrix $\mathbf{H}$, returns the desired transmitted signal $\mathbf{x}$. This can be formulated as the least squares solution to a system of linear equations

$$\hat{\mathbf{y}} = \underset{\mathbf{y}}{\operatorname{argmin}} ||\mathbf{H}\mathbf{y} - \mathbf{x}||^2. \tag{24}$$

It is obvious that, if the the channel matrix $\mathbf{H}$ is squared and invertible, the solution is obtained by matrix inversion $\hat{\mathbf{y}} = \mathbf{H}^{-1}\mathbf{x}$, and the zero forcing precoding matrix is simply $\mathbf{U}_{\mathrm{ZF}} = \mathbf{H}^{-1}$. The signal to be transmitted is multiplied by the inverse of the channel matrix; the precoding acts as a form of "spatial equalizer" such that the cascade of the precoder and channel matrix returns an "equalized" channel for each user. By doing so, the effect of noise is completely neglected creating detrimental effects at low Signal-to-Noise Ratios (SNRs). For non-squared channel matrices the solution of the optimization problem (24) can be obtained as the stationary point of the cost function to be minimized resulting in the linear solution, $\hat{\mathbf{y}} = \mathbf{U}_{\mathrm{ZF}}\mathbf{x}$, where

$$\mathbf{U}_{\mathrm{ZF}} = \left(\mathbf{H}^H\mathbf{H}\right)^{-1}\mathbf{H}^H. \tag{25}$$

This expression, often reported in MIMO and multiuser detection literature, is defined only in case the matrix $\mathbf{H}$ is "tall" (i.e. the number of rows exceeds the number of columns) and full rank (i.e. the Gram matrix $\mathbf{H}^H\mathbf{H}$ is invertible). It is also known as the left pseudo-inverse of $\mathbf{H}$, as it generalizes the inversion of "tall" full-rank matrices as solution of the least-squares over-determined linear system (24). When the matrix $\mathbf{H}$ is not full-rank we must resort to the more powerful Moore-Penrose pseudo inverse [24], [25] which is a unique generalization of the matrix inversion operation. In the following, the Moore-Penrose pseudo inverse will be indicated with a the $^+$ superscript. The general ZF precoding matrix can be thus expressed as the Moore-Penrose pseudo inverse of the channel matrix

$$\mathbf{U}_{\mathrm{ZF}} = \mathbf{H}^{+}, \tag{26}$$

or derived following (25) using the Moore-Penrose pseudo inverse for the inversion of the Gram matrix $\mathbf{H}^H\mathbf{H}$

$$\mathbf{U}_{\mathrm{ZF}} = \left(\mathbf{H}^H\mathbf{H}\right)^{+}\mathbf{H}^H. \tag{27}$$

While (27) is well posed, it hides an intrinsic computational complexity due to the large size and rank deficiency of the Gram matrix $\mathbf{H}^H\mathbf{H}$. An equivalent, yet more efficient form, is discussed in Annex A.

4) MINIMUM MEAN SQUARE ERROR

Linear Minimum Mean Square Error (L-MMSE) methods have been first elaborated and developed in the area of linear detection. They are formulated as the solution to the problem of evaluating a linear matrix operator that minimizes some statistical error metrics between the transmitted quantities and their observations. Due to the statistical nature of the optimization problem, knowledge of the the covariance matrices of the transmitted signal and noise is necessary. In the hypothesis of independent and identically distributed (IID) random variables, the optimal linear detector has the form

$\left(\mathbf{H}^H\mathbf{H}+\mathbf{I}\right)^{-1}\mathbf{H}^H$. Broadly speaking, precoding matrices of the type

$$\mathbf{U}_{\mathrm{MMSE}} = \left(\mathbf{H}^H\mathbf{H}+\lambda\mathbf{I}\right)^{-1}\mathbf{H}^H, \tag{28}$$

are indicated as linear MMSE precoders. The derivation of (28) and the choice of the optimal λ parameter depends on the formulation of the optimization problem. In non-statistical terms, the solution (28) can be considered a regularized version of the left pseudo-inverse (25) where the $\lambda\mathbf{I}$ term is added as a perturbation to the Gram matrix $\mathbf{H}^H\mathbf{H}$ to render it invertible. Optimization of λ according to a Signal to Noise plus Interference (SNIR) criteria is described in [26]. A derivation of (28) as a power constrained MMSE transmit filter is reported in [27] where λ is the Lagrange multiplier associated to the power constraint. The close relationship to the MMSE detector is demonstrated in the uplink-downlink duality framework developed for characterizing the sum capacity of the Gaussian Broadcast channel [28] and the resulting optimality condition, $\lambda = 1$, will be used in the rest of the paper. While the MMSE precoder (28) does not suffer of rank deficiency, the complexity of its evaluation resides in the size and of the Gram matrix $\mathbf{H}^H\mathbf{H}$ which derives from a ''fat'' (i.e. the number of columns exceeds the number of rows) channel matrix $\mathbf{H}$. An equivalent, yet more efficient form, is discussed in Annex A.

D. PRECODING MATRICES NORMALIZATION

The normalization of the precoding/beamforming matrix plays an important role in properly accounting for practical payload limitations such as the per antenna element power limitation affecting the DRA architecture (see Fig. 1). The evaluation of $\mathbf{U}$ according to the principles described in Sec. II-C, does not satisfies any normalization or power constraints criteria. A normalised precoding/beamforming matrix $\hat{\mathbf{U}}$ can then be introduced as

$$\hat{\mathbf{U}} = \begin{bmatrix} \hat{u}(1,1) & \cdots & \hat{u}(1,N_U) \\ \vdots & & \vdots \\ \hat{u}(N_T,1) & \cdots & \hat{u}(N_T,N_U) \end{bmatrix}. \tag{29}$$

The normalised precoding/beamforming matrix $\hat{\mathbf{U}}$, similarly to the un-normalised matrix $\mathbf{U}$, can be decomposed in column vectors

$$\hat{\mathbf{U}} = \left[\hat{\mathbf{u}}^{\mathrm{C}}_1 \quad \cdots \quad \hat{\mathbf{u}}^{\mathrm{C}}_{N_U}\right], \tag{30}$$

where the j-th column vector represents the array complex weights for the j-th user and is given by

$$\hat{\mathbf{u}}^{\mathrm{C}}_j = \begin{bmatrix} \hat{u}(1,j) \\ \vdots \\ \hat{u}(N_T,j) \end{bmatrix}. \tag{31}$$

Alternatively, $\hat{\mathbf{U}}$ can be decomposed in row vectors as

$$\hat{\mathbf{U}} = \begin{bmatrix} \hat{\mathbf{u}}^{\mathrm{R}}_1 \\ \vdots \\ \hat{\mathbf{u}}^{\mathrm{R}}_{N_T} \end{bmatrix}, \tag{32}$$

where the n-th array component is given by

$$\hat{\mathbf{u}}^{\mathrm{R}}_n = \left[\hat{u}(n,1) \quad \cdots \quad \hat{u}(n,N_U)\right]. \tag{33}$$

Assuming the input signals of normalised unitary power, the beamforming delivered power for user j with $1 \le j \le N_U$ can be computed as

$$\left|\left|\hat{\mathbf{u}}^{\mathrm{C}}_j\right|\right|^2 = \sum_{n=1}^{N_T} |\hat{u}(n,j)|^2. \tag{34}$$

Similarly the beamforming delivered power for antenna element n with $1 \le n \le N_T$ can be computed as

$$\left|\left|\hat{\mathbf{u}}^{\mathrm{R}}_n\right|\right|^2 = \sum_{j=1}^{N_U} |\hat{u}(n,j)|^2. \tag{35}$$

Depending on the power constraints, per user or per antenna element, normalisation of the precoding/beamforming matrix columns or rows have been introduced. To have a common framework for the normalization we introduce a normalization of the precoding/beamforming matrix to its Frobenius norm defined as the square root of the sum of the absolute squares of its elements. The overall precoding matrix squared norm is then

$$\begin{aligned} \left|\left|\hat{\mathbf{U}}\right|\right|^2_F &= \sum_{i=1}^{N_T}\sum_{j=1}^{N_U} |\hat{u}(i,j)|^2 \\ &= \sum_{j=1}^{N_T}\left|\left|\hat{\mathbf{u}}^{\mathrm{R}}_j\right|\right|^2 = \sum_{i=1}^{N_U}\left|\left|\hat{\mathbf{u}}^{\mathrm{C}}_i\right|\right|^2 \le 1, \end{aligned} \tag{36}$$

such that for a total satellite DRA RF power per carrier P^c_T (where it is assumed that the total DRA available RF power is equally distributed among the frequency slot carriers) the transmitted RF power per TDM carrier will be $P^c = P^c_T\left|\left|\hat{\mathbf{U}}\right|\right|^2_F \le P^c_T$. Similarly we have that the RF power for the j-th user transmitted by the array is $P_j = P^c_T\left|\left|\hat{\mathbf{u}}^{\mathrm{C}}_j\right|\right|^2$, and the power transmitted by the n-th antenna element is $P_n = P^c_T\left|\left|\hat{\mathbf{u}}^{\mathrm{R}}_n\right|\right|^2$. The evaluation of the precoding/beamforming matrix $\mathbf{U}$ according to Sec. II-C principles does not satisfies normalization or power constraints criteria and different strategies can be applied to normalise it while enforcing relevant power constraints.

1) TARICCO'S PER USER AND ANTENNA ELEMENT POWER NORMALIZATION

The following MIMO precoding matrix normalization was proposed by Taricco in [6] for more conventional single feed per beam payload. This normalization was inspired by [11] to ensure that all the active users get the same RF power while the per radiating element power limitation is not violated. Analytically this can be formulated as a first normalization such that all the users are allocated and identical transmit power as

$$\tilde{\mathbf{U}} = \frac{1}{\sqrt{N_T}}\mathbf{U}\,\mathrm{diag}\left\{\frac{1}{||\mathbf{u}^{\mathrm{C}}_1||},\cdots,\frac{1}{||\mathbf{u}^{\mathrm{C}}_{N_U}||}\right\}, \tag{37}$$

and as a second rescaling such that the power per rows does not exceed the available power per antenna element

$$\hat{\mathbf{U}} = \text{diag}\left\{\sigma_1, \cdots, \sigma_{N_T}\right\}\tilde{\mathbf{U}}, \tag{38}$$

with σ_n, $1 \leq n \leq N_T$, derived as

$$\begin{cases} 1 & \text{if } ||\tilde{\mathbf{u}}_n^{\mathrm{R}}|| \leq \dfrac{1}{\sqrt{N_T}} \\ \dfrac{1}{\sqrt{N_T}||\tilde{\mathbf{u}}_n^{\mathrm{R}}||} & \text{if } ||\tilde{\mathbf{u}}_n^{\mathrm{R}}|| > \dfrac{1}{\sqrt{N_T}}. \end{cases} \tag{39}$$

2) TARICCO'S MODIFIED PER USER AND ANTENNA ELEMENT POWER NORMALIZATION

This approach, proposed here by the authors, ensures that while the same power is assigned to each user, the DRA power per element is fully exploited at least for the highest value element which was not the case for the original Taricco's formulation, at least for the case of M-MIMO where $N_T > N_U$. The first normalization step is the same as in the previous approach. Instead, the second step (38) is implemented in two sub-steps as

$$\sigma_n^* = \begin{cases} 1 & \text{if } ||\tilde{\mathbf{u}}_n^{\mathrm{R}}|| \leq \dfrac{1}{\sqrt{N_T}} \\ \dfrac{1}{\sqrt{N_T}||\tilde{\mathbf{u}}_n^{\mathrm{R}}||} & \text{if } ||\tilde{\mathbf{u}}_n^{\mathrm{R}}|| > \dfrac{1}{\sqrt{N_T}}, \end{cases}$$

$$\sigma_n = \begin{cases} \sigma_n^* & \text{if } \max\limits_p \left\|\tilde{\mathbf{u}}_p^{\mathrm{R}}\right\| \geq \dfrac{1}{\sqrt{N_T}} \\ \dfrac{1}{\sqrt{N_T}\max\limits_p \left\|\tilde{\mathbf{u}}_p^{\mathrm{R}}\right\|} & \text{if } \max\limits_p \left\|\tilde{\mathbf{u}}_p^{\mathrm{R}}\right\| < \dfrac{1}{\sqrt{N_T}}. \end{cases} \tag{40}$$

In this way we enforce that the $\hat{\mathbf{U}}$ precoding/beamforming matrix largest antenna element norm is equal to $1/\sqrt{N_T}$. This ensures that the DRA power dynamic is fully exploited.

3) CTTC'S PER USER AND ANTENNA ELEMENT POWER NORMALIZATION

This approach was recently proposed in [35] as a variation of the Taricco's normalization proposal. The main difference is that after normalizing the $\mathbf{U}$ precoding matrix per user is also normalizing per antenna element norm for all elements to exploit all the RF power available in the DRA at the expenses of the co-channel interference mitigation. Also in this case the first step corresponds to a normalization of the columns to a constant power per user (37), while for the second step (38) is implemented with σ_n, $1 \leq n \leq N_T$, derived as

$$\sigma_n = \frac{1}{\sqrt{N_T}||\tilde{\mathbf{u}}_n^{\mathrm{R}}||}, \tag{41}$$

which corresponds to a normalization of all the row vectors to $1/\sqrt{N_T}$.

E. FIGURES OF MERIT CALCULATIONS

1) POWER TRANSFER, SNR, INR, AND SNIR CALCULATIONS

The units and the normalisation of the channel matrix $\mathbf{H}$ and of the precoding/beamforming matrix $\hat{\mathbf{U}}$ are such that we can evaluate the power transmitted for the user j and received by the user i, normalised to the noise power, as the power transfer coefficient $s(i,j)$ computed as $s(i,j) = P_T^c \left|\mathbf{h}_i^{\mathrm{R}}\,\hat{\mathbf{u}}_j^{\mathrm{C}}\right|^2$, which can be arranged in a $(N_U \times N_U)$ normalised power transfer matrix $\mathbf{S}$ with elements

$$\mathbf{S} = \begin{bmatrix} s(1,1) & \cdots & s(1,N_U) \\ \vdots & & \vdots \\ s(N_U,1) & \cdots & s(N_U,N_U) \end{bmatrix}. \tag{42}$$

Introducing the element-wise absolute square matrix operator $|\cdot|^2$ so that $\mathbf{B} = |\mathbf{A}|^2$ returns a matrix $\mathbf{B}$ of the same dimension of $\mathbf{A}$ and entries equal to the absolute square of the entries of $\mathbf{A}$, $b(i,j) = |a(i,j)|^2$, we can write $\mathbf{S} = P_T^c \left|\mathbf{H}\hat{\mathbf{U}}\right|^2$.

Recalling (1), the M-MIMO signal-to-noise, interference-to-noise and signal-to-noise plus interference ratio for the i-th user can be derived from relevant entries of the matrix $\mathbf{S}$, respectively

$$\text{SNR}^{\mathrm{M}}(i) = s(i,i), \quad \text{INR}^{\mathrm{M}}(i) = \sum_{j=1,\, j\neq i}^{N_U} s(i,j), \tag{43}$$

$$\text{SNIR}^{\mathrm{M}}(i) = \frac{s(i,i)}{1 + \sum\limits_{j=1,\, j\neq i}^{N_U} s(i,j)} = \frac{\text{SNR}^{\mathrm{M}}(i)}{1 + \text{INR}^{\mathrm{M}}(i)}. \tag{44}$$

Thus the diagonal entries of the matrix $\mathbf{S}$ represent the useful part of the transmission corresponding to the signal-to-noise-ratio. All the off-diagonal elements are unwanted contributions that should be minimised. Taking the elements of the i-th row, with the exclusion of the diagonal one, we get the aggregate interference-to-noise ratio experienced by the i-th user. While taking the i-th column, the off-diagonal elements represent the power of the patterns for the i-th user leaking in undesired directions normalized to the noise power. The matrix $\mathbf{S}$ is generally non-symmetric.

2) THROUGHPUT CALCULATION

The system throughput can be derived from the signal-to-noise plus interference ratio experienced by user i derived in (44). The average system throughput calculation $\overline{T}$ is computed as the expectation over the N_{trials} users' realization of the aggregated throughput $\sum_{i=1}^{N_U} T(i)$ summing all users' throughput contributions at each Monte Carlo realization of the users' distribution over the ROI. This can be formulated as

$$\overline{T} = E\left\{\sum_{i=1}^{N_U} T(i)\right\}, \tag{45}$$

where the i-th user Shannon throughput is simply computed as $T^{\mathrm{S}}(i) = R_s \log_2(1 + \text{SNIR}(i))$. Instead, assuming the use of the DVB-S2X standard [9], the i-th user throughput is derived as $T^{\mathrm{S2X}}(i) = R_s\ \eta_{\mathrm{S2X}}(\text{SNIR}(i))$, where the function η_{S2X} maps the DVB-S2X standard [9] spectral efficiency as a function of the individual user SNIR dubbed SNIR_i. The details about the η_{S2X} function can be derived from [9].

3) OUTAGE PROBABILITY CALCULATION

The outage probability[4] for a specific M-MIMO or beamforming technique is simply derived as $N_{\text{out}}/N_{\text{TOT}}$ where N_{out} corresponds to the number of events for which $\text{SNIR}_i < \text{SNIR}_{\text{min}}$. The minimum SNIR value SNIR_{min} corresponds to the minimum signal-to-noise plus interference ratio at which the adaptive physical layer can decode a frame with acceptable frame error rate probability. N_{TOT} represents the total number of simulated link events i.e. $N_{\text{TOT}} = N_U\ N_{\text{trials}}$, where N_{trials} corresponds to the number of Monte Carlo trials.

F. COLOUR FREQUENCY REUSE

In the above formulation applicable to the M-MIMO case it has been assumed that all the active users share the same frequency and polarization and said resource has been indicated as carrier. The active antenna RF power available for the carrier under consideration is termed P_T^c. In general, the satellite payload may transmit an integer number of carriers in the allocated bandwidth and polarization(s) and the total satellite RF power P_T must be split between the carriers. The Sec. II-C2 beam assignment formulation can be extended to the more conventional case of multibeam satellite systems with colour frequency reuse allowing a seamless assessment of system throughput and outage performance. As per Sec. II-C2, we can consider an hexagonal lattice of beams generated by an hexagonal lattice base matrix $\boldsymbol{S}_{\text{MB}}$ with beam-to-beam inter-distance defined by the normalised beam spacing S_{MB}^n. While the overall lattice $\Lambda(\boldsymbol{S}_{\text{MB}})$ is infinite, the N_B useful beams are defined by the set of beams centers within the u, v disk of radius $\sin(\vartheta_{\text{max}})$ as per (21).

Considering that the co-frequency beams satisfy periodicity conditions, we can use the mathematical tool of sub-lattices to identify co-frequency beams. A sub-lattice of $\Lambda(\boldsymbol{S}_{\text{MB}})$ can be defined by mean of an integer non-singular matrix M and is given by

$$\Lambda(\boldsymbol{S}_{\text{MB}}\text{M}) = \Lambda(\boldsymbol{S}_{\text{MB}})\text{M}. \tag{46}$$

The matrix $\boldsymbol{S}_{\text{MB}}\text{M}$ plays the role of a vectorial base for the lattice $\Lambda(\boldsymbol{S}_{\text{MB}}\text{M})$, which for our purposes will identify the lattice of beams sharing the same frequency with the one at the origin.[5] Given $\boldsymbol{S}_{\text{MB}}\text{M}$, it is possible to introduce the "vectorial modulo" operation [29]. Two vectors in $\Lambda(\boldsymbol{S}_{\text{MB}})$ are said to be congruent modulo $\boldsymbol{S}_{\text{MB}}\text{M}$ if their difference belongs to $\Lambda(\boldsymbol{S}_{\text{MB}})$. The vectorial modulo operation can be used to induce on $\Lambda(\boldsymbol{S}_{\text{MB}})$ a set of equivalence classes in number equal to $|\det(\text{M})|$, called the index of $\Lambda(\boldsymbol{S}_{\text{MB}})$ in $\Lambda(\boldsymbol{S}_{\text{MB}}\text{M})$. Each equivalence class is a shifted version of $\Lambda(\boldsymbol{S}_{\text{MB}}\text{M})$. For further details refer to [30].

[4]Because of having neglected the atmospheric fading attenuation as per Sec. II-B4, the M-MIMO outage refers to AWGN and co-channel interference effects only.

[5]For simplicity we will consider the lattice of beams having a central beam pointing at the center of the u, v coordinates. A different configuration is easily obtained by mean of a trivial translation and will not be discussed further.

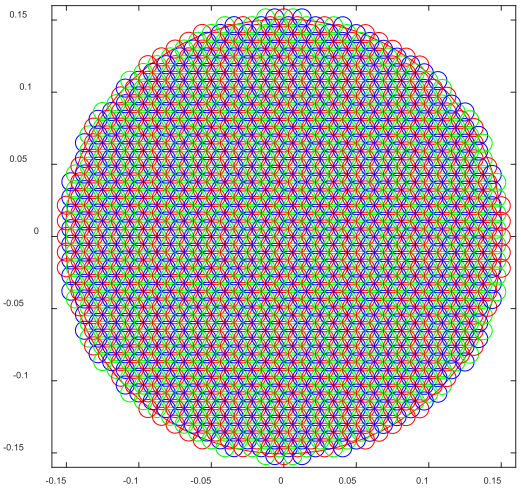

FIGURE 7. Three colours beam lattice.

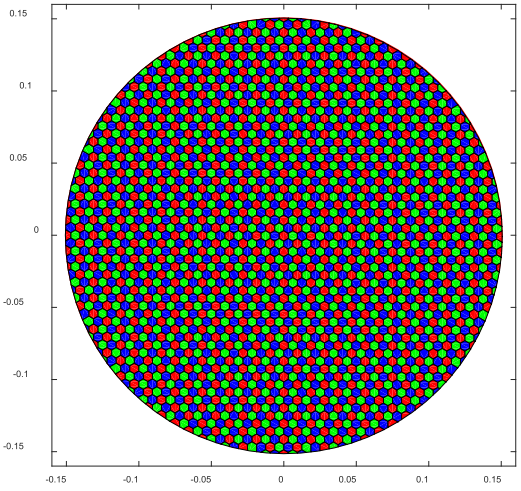

FIGURE 8. Three colours coverage assignment.

In the present context $|\det(\text{M})|$ identifies the number of different colours N_C, $N_C = |\det(\text{M})|$, and M the colouring base. Two beams of the lattice $\Lambda(\boldsymbol{S}_{\text{MB}})$ with pointing direction $\boldsymbol{s}_k$ and $\boldsymbol{s}_l$ are co-frequency if and only if $(\boldsymbol{s}_k - \boldsymbol{s}_l)$ mod $(\boldsymbol{S}_{\text{MB}}\text{M}) = \boldsymbol{0}$, As an example, the following non unique colouring bases M_3 and M_4 generates 3 and 4 colours frequency reuse patterns:

$$\text{M}_3 = \begin{bmatrix} 1 & -1 \\ 1 & 2 \end{bmatrix}, \quad \text{M}_4 = \begin{bmatrix} 2 & 0 \\ 0 & 2 \end{bmatrix}. \tag{47}$$

Figures 7 and 8 show beam lattices associated to the M_3 and M_4 colouring bases. The lattices correspond to a normalised beam spacing $S_{\text{MB}}^n = 0.5$ for an array size $D_A = 1.2$ m. Relevant coverage assignment based on best gain criteria is shown in Figures 9 and 10, respectively.

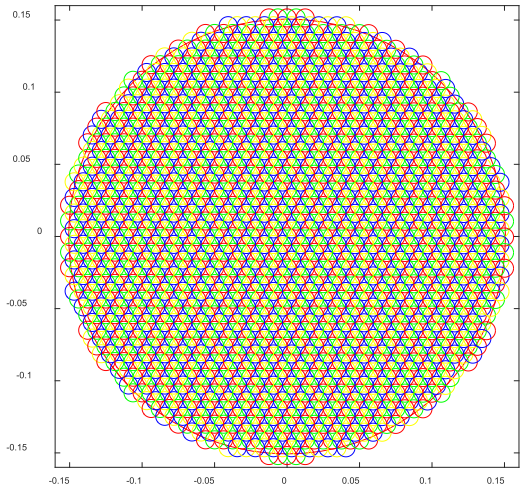

FIGURE 9. Four colours beam lattice.

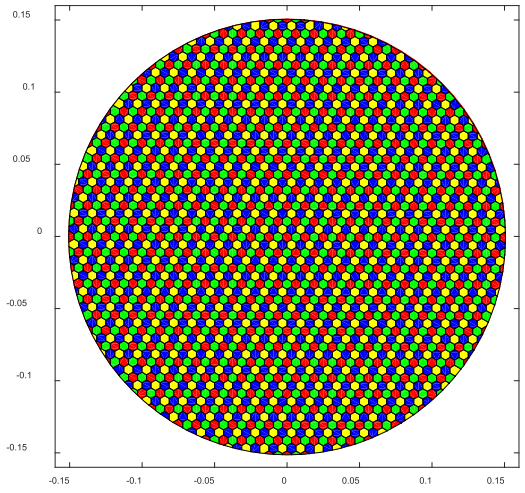

FIGURE 10. Four colours coverage assignment.

The precoding/beamforming matrix generating the beam lattice is described by the $(N_T \times N_B)$ phase matrix

$$\mathbf{U}_{\mathrm{CFR}} = \begin{bmatrix} u_{\mathrm{CFR}}(1,1) & \cdots & u_{\mathrm{CFR}}(1,N_B) \\ \vdots & & \vdots \\ u_{\mathrm{CFR}}(N_T,1) & \cdots & u_{\mathrm{CFR}}(N_T,N_B) \end{bmatrix}, \quad (48)$$

where the generic (n,k) entry element is $u_{\mathrm{CFR}}(n,k) = \exp(-jk_0\,\boldsymbol{r}_n \cdot \boldsymbol{s}_k)$.

We can now assume that for the k-th beam, COL(k) represents the assigned colour number, $1 \le c \le N_C$, and we can introduce a beam colouring matrix $\mathbf{C}_B$ of size $(N_B \times N_C)$ with binary entries

$$\mathbf{C}_B = \begin{bmatrix} c_B(1,1) & \cdots & c_B(1,N_C) \\ \vdots & & \vdots \\ c_B(N_B,1) & \cdots & c_B(N_B,N_C) \end{bmatrix}, \quad (49)$$

where

$$c_B(k,l) = \begin{cases} 1 & \text{if COL}(k) = l \\ 0 & \text{otherwise.} \end{cases} \quad (50)$$

The matrix product of $\mathbf{C}_B$ with its transpose $\mathbf{C}_B{}^T$ generates the co-frequency beam matrix $\mathbf{X}_B$ of size $(N_B \times N_B)$ whose binary entries are true if the beams corresponding to the row and column indexes share the same frequency. The matrix $\mathbf{C}_B$ can be computed as $\mathbf{X}_B = \mathbf{C}_B\mathbf{C}_B{}^T$, with

$$\mathbf{X}_B = \begin{bmatrix} x_B(1,1) & \cdots & x_B(1,N_B) \\ \vdots & & \vdots \\ x_B(N_B,N_B) & \cdots & x_B(N_B,N_B) \end{bmatrix}, \quad (51)$$

where

$$x_B(p,q) = \begin{cases} 1 & \text{if COL}(p) = \text{COL}(q) \\ 0 & \text{otherwise.} \end{cases} \quad (52)$$

The matrix $\mathbf{X}_B$ is symmetric with unit diagonal elements and can be used in conjunction with the user-to-beam assignment function BEAM(i) to identify co-frequency users. For this purpose, we need to map the co-frequency beam matrix $\mathbf{X}_B$ of size $(N_B \times N_B)$ in a co-frequency user matrix $\mathbf{X}_U$ of size $(N_U \times N_U)$ described as

$$\mathbf{X}_U = \begin{bmatrix} x_U(1,1) & \cdots & x_U(1,N_U) \\ \vdots & & \vdots \\ x_U(N_U,1) & \cdots & x_U(N_U,N_U) \end{bmatrix}, \quad (53)$$

The mapping of $\mathbf{X}_B$ in $\mathbf{X}_U$ consists in assigning to $x_U(i,j)$ the value of $x_B(p,q)$ with $p = \text{BEAM}(i)$ and $q = \text{BEAM}(j)$, computed as

$$\begin{aligned} x_U(i,j) &= x_B(\text{BEAM}(i), \text{BEAM}(j)) \\ &= \begin{cases} 1 & \text{if COL}(\text{BEAM}(i)) = \text{COL}(\text{BEAM}(j)) \\ 0 & \text{otherwise} \end{cases} \end{aligned} \quad (54)$$

In other words, the element $x_U(i,j)$ of the co-frequency user matrix $\mathbf{X}_U$ is equal to one when the i-th user and the j-th user are assigned to co-frequency beams, zeros otherwise. The co-frequency user matrix $\mathbf{X}_U$ is itself a symmetric matrix with unit diagonal elements and has the same dimensions of the power transfer matrix $\mathbf{S}$. They can be combined by mean of the Hadamard product in a resulting co-frequency power transfer matrix $\mathbf{S}_{\mathrm{CFR}}$ which takes into account frequency assignments. The matrix $\mathbf{S}_{\mathrm{CFR}}$ can be computed as

$$\mathbf{S}_{\mathrm{CFR}} = \mathbf{X}_U \odot \mathbf{S}. \quad (55)$$

The CFR signal-to-noise, interference-to-noise and signal-to-noise plus interference ratio for the i-th user can be derived from relevant entries of the matrix $\mathbf{S}_{\mathrm{CFR}}$, respectively as

$$\begin{aligned} &\mathrm{SNR}^{\mathrm{C}}(i) = s(i,i), \quad \mathrm{INR}^{\mathrm{C}}(i) = \sum_{j=1,\, j\neq i}^{N_U} x_U(i,j)s(i,j), \\ &\mathrm{SNIR}^{\mathrm{C}}(i) = \frac{s(i,i)}{1 + \sum\limits_{j=1,\, j\neq i}^{N_U} x_U(i,j)s(i,j)} = \frac{\mathrm{SNR}^{\mathrm{C}}(i)}{1 + \mathrm{INR}^{\mathrm{C}}(i)}. \end{aligned} \quad (56)$$

It is worth noting that to be coherent with the normalization of the precoding/beamforming matrix $||\hat{\mathbf{U}}||_F^2$, and considering that the normalised matrix $\hat{\mathbf{U}}$ collects the steering vectors of all the active beams for all the considered colours, the power transfer coefficient $s(i,j)$ must account for the total available power P_T for the set of considered colours as follows

$$s(i,j) = P_T \left| \mathbf{h}_i^{\mathrm{R}} \, \hat{\mathbf{u}}_j^{\mathrm{C}} \right|^2, \quad \mathbf{S} = P_T \left| \mathbf{H}\hat{\mathbf{U}} \right|^2. \tag{57}$$

The total capacity for the set of considered beams and colours can be evaluated according to the formulation in Sec. II-E2.

G. RADIO RESOURCE MANAGEMENT ASPECTS

The formulation developed for the assessment of the system performance with a coloured frequency assessment constitutes an useful framework for addressing the general problem of resource management in a M-MIMO system and is prone to further generalisations. An overview of RRM research aspects for terrestrial Multi User MIMO systems is reported in [31]. Reference [32] goes in the direction of separating users for a satellite multi-beam system with precoding. However, the proposed approach is applicable to a single feed multi-beam system, thus, not to a M-MIMO one. Furthermore, the proposed solution is based on geometric considerations related to the beam configuration which allows to implement the proposed beam sectorization approach. In our M-MIMO system there is no notion of beam therefore this approach is not applicable. Finally, the approach described in [32] is heuristic and, as such, does not guarantee to be overall optimal (e.g. in the instances of random selection of unused resources within the allocation algorithm).

In a real operational scenario, the user distribution is an uncontrollable input with non-uniform statistical distribution and possible clustering due to hot spots in areas of high user density. Still the users can be assigned to different radio resources (time slots and/or frequency carriers) in a manner that maximise the overall throughput. On one hand, analysing the power transfer matrix $\mathbf{S}$, it can be easily recognised that the off-diagonal coefficients $s(i,j)$ play a detrimental effect in increasing the interference experienced by the i-th user. M-MIMO techniques aim at reducing the interference by properly shaping the precoding matrix $\hat{\mathbf{U}}$ but, especially for closely spaced users, the precoding has reduced efficiency due to the limited antenna resolution capability and to the detrimental effect on the wanted user gain. On the other hand, assigning the users to different time/frequency slots nulls their reciprocal interference. As shown in Sec. II-F, this effect can be modelled with a generalised co-channel matrix $\mathbf{X}$ for which a unit entry identifies the assignment of the same resource to the users with relevant row and column indexes.

Given a power transfer matrix $\mathbf{S}$ the resource management problem can be cast in a colour assignment problem (in terms of time[6] or frequency resources) which for numerical tractability is formulated as a 0-1 integer programming instance on the colouring matrix binary entries. We will consider the number of colours C preassigned such that the binary colouring matrix $\mathbf{C}$ is of size $(N \times C)$, with N the total number of users[7]

$$\mathbf{C} = \begin{bmatrix} c(1,1) & \cdots & c(1,C) \\ \vdots & & \vdots \\ c(N,1) & \cdots & c(N,C) \end{bmatrix}, \tag{58}$$

considering that the i-th user can be assigned only to one colour, the rows of $\mathbf{C}$ must satisfy the following linear constraint corresponding to one user per colour

$$\sum_{c=1}^{C} c(i,c) = 1 \quad \forall\, i. \tag{59}$$

The matrix product of $\mathbf{C}$ with its transpose $\mathbf{C}^T$ generates the co-channel matrix $\mathbf{X}$ of size $(N \times N)$ with unit entries if the users corresponding to the row and column indexes share the same colour $\mathbf{X} = \mathbf{C}\mathbf{C}^T$. Considering that the central target of the colour assignment is the reduction of the mutual interference we focus our attention on the off-diagonal elements of the power transfer matrix introducing its diagonally null part $\mathbf{Q}$ which we briefly term the interference matrix as

$$\mathbf{Q} = \mathbf{S} - \mathrm{diag}\left\{\mathrm{diag}(\mathbf{S})\right\}, \quad q(i,j) = \begin{cases} 0 & \text{if } i = j \\ s(i,j) & \text{if } i \neq j. \end{cases} \tag{60}$$

where the diag $\{\cdot\}$ operator is used accordingly to MATLAB notation (i.e. returning a vector with the diagonal elements of a square matrix, and returning a diagonal square matrix if applied to a vector). The co-channel matrix $\mathbf{X}$ acts on the interference matrix $\mathbf{Q}$ as selector of the co-channel interference entries. Their Hadamard product, $\mathbf{X} \odot \mathbf{Q}$, returns the co-channel interference contributions that must be accounted for in the interference-to-noise ratio (INR) performance assessment as

$$\mathrm{INR}(i) = \sum_{j=1}^{N} x(i,j) q(i,j). \tag{61}$$

The aggregated co-channel interference, evaluated as the total interference-to-noise ratio INR_T, can be assumed as a figure of merit of the overall performance and satisfies the following definition

$$\mathrm{INR}_T = \sum_{i=1}^{N} \mathrm{INR}(i) = \sum_{i=1}^{N} \sum_{j=1}^{N} x(i,j) q(i,j). \tag{62}$$

In matrix form we can write INR_T as $\mathrm{INR}_T = \mathbf{1}^T (\mathbf{Q} \odot \mathbf{X}) \mathbf{1}$, where the $(N \times 1)$ vector $\mathbf{1}$ has all unit entries. Vectorizing the matrix $\mathbf{C}$ of size $(N \times C)$ into a column vector, vec$(\mathbf{C})$, of size $(NC \times 1)$ obtained by stacking the columns of $\mathbf{C}$ on top of each other as

$$\mathrm{vec}(\mathbf{C}) = [c(1,1), \ldots, c(N,1), \ldots, c(1,C), \ldots, c(N,C)]^T,$$

[6]Resources TDM time slicing is the preferred approach for M-MIMO where full frequency reuse is assumed.

[7]Not to be confused with the number of active users $N_U < N$.

(63)

and exploiting some matrix identities, we can formulate the aggregated co-channel interference as a quadratic form on the column vector vec(**C**) (see Appendix B for details) as

$$\mathrm{INR}_T = \mathrm{tr}\left(\mathbf{C}^T\mathbf{Q}\mathbf{C}\right) = (\mathrm{vec}(\mathbf{C}))^T\,(\mathbf{I}\otimes\mathbf{Q})\,\mathrm{vec}(\mathbf{C}).$$

The resource management problem can be thus cast in a Mixed Integer Quadratic Programming (MIQP) problem with the form

$$\begin{aligned}&\text{minimize}\ \ [\mathrm{vec}(\mathbf{C})]^T\,(\mathbf{I}\otimes\mathbf{Q})\,\mathrm{vec}(\mathbf{C})\\ &\text{subject to}\ \sum_{j=1}^{C} c(i,j)=1,\quad c(i,j)\in\{0,1\},\qquad \begin{matrix} i=1,...,N,\\ j=1,...,C.\end{matrix}\end{aligned} \tag{64}$$

Several techniques have been proposed for solving in exact or sub-optimal manner MIQP problems. An efficient heuristic approach has been proposed in [33] in the context of a beam colouring problem which can be easily extended to the present general problem.

Some comment is now in order regarding the self-consistency of the optimization. In particular, it should be noted that the matrix **Q**, which collects the mutual interference terms, is evaluated on the basis of a given precoding/beamforming matrix. For ZF and MMSE, the precoding accounts for the co-channel interference, thus the resource management and precoding calculation results to be interlinked. A possible approach would consist in an iterative optimization of the precoding and resource management. However, its convergence is not guaranteed and additional complexity is added to the precoding evaluation process. Instead, for the MF and MB approaches, which take into account only the information on the desired user (i.e. channel matrix row and user position, respectively), the precoding/beamforming evaluation and the resource management are decoupled problems that can be solved independently.

Finally, an a priori evaluation of the interference matrix **Q** based on the mutual distance is possible and is proposed as an effective solution to the resource management problem. Neglecting the element gain variation $g_E(u, v)$ in equation (5) and considering the uniform tapering with the normalised array complex weights $\mathbf{w} = \mathbf{1}/\sqrt{N_T}$ where the $(N_T \times 1)$ vector **1** has all unit entries, using equations (4), (5) and (14) we can introduce a normalised array gain $g_A(u, v)$ for the nadir prototype beam as

$$g_A(u,v) = \frac{1}{\sqrt{N_T}}\sum_{n=1}^{N_T}\exp\left[jk_0(x_n u + y_n v)\right]. \tag{65}$$

The normalised interference term $q_0(i, j)$ can be thus evaluated as

$$q_0(i,j) = \left|g_A(u_i-u_j, v_i-v_j)\right|^2. \tag{66}$$

Considering that the strong mutual interference is due to close spacing of the users, a Gaussian beam pattern approximation, with 4 dB beam-width corresponding to the the array D_A/λ can be used. Alternatively, antenna masks based on different beam zones (main beam, first sidelobes, far sidelobes) have been proposed in [34] and can also be adopted to model the interference dependency on the antenna pattern.

In the following, we adopted a further interference model simplification to derive a RRM approach dubbed Minimum Distance MIQP (MD-MIQP RRM). We assume that the co-channel interference is dominated by the adjacent beams pattern which envelope is related to the users distance with an intensity inversely proportional to the squared distance.[8] As a consequence, the RRM optimization aims to guarantee that the normalized users' minimum distance $\rho_{\min}$ is larger than a value to be experimentally derived by optimizing the throughput. Once this optimum $\rho_{\min}$ value has been found we will also know the number of user which can be simultaneously served per slice, thus the number of (time) slices required to serve the overall users' population.

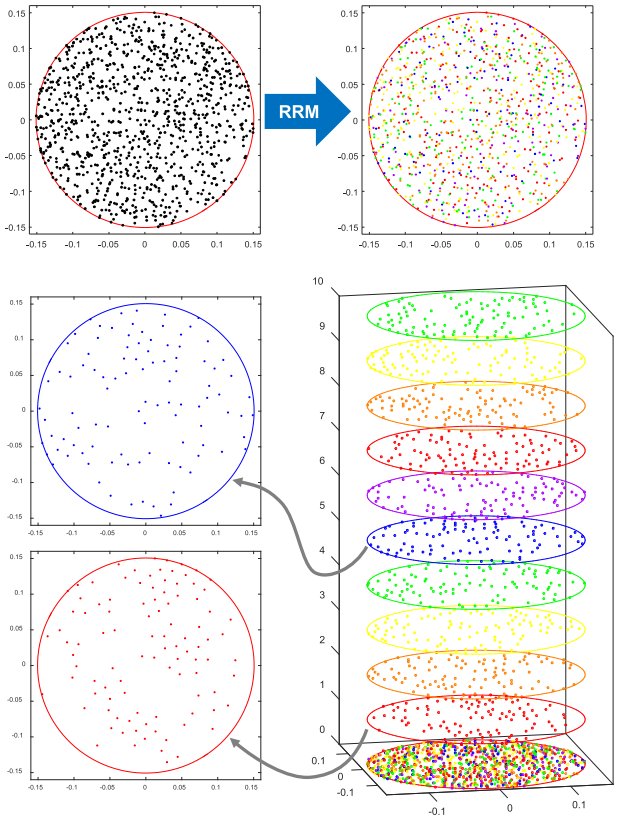

FIGURE 11. Example time slicing by means of MD-MIQP RRM.

An example of resource slicing with the proposed MD-MIQP RRM is shown in Fig. 11 for a number of colours (time slices) $C = 10$. The algorithm is run on a population

[8]The validity of this approximation is linked to the decay of sidelobes of radiation patterns of uniformly illuminated apertures. As an example, the voltage pattern of an uniform linear aperture of size D_A is $\sin(k_0\, uD_A)/(k_0\, u)$. Due to the limitedness of the oscillating sinusoidal term, the power pattern envelope is bounded by $1/(k_0\, u)^2$, which is consistent with the inversely squared distance proportionality.

TABLE 1. Simulation system parameters.

Parameter	Symbol	Value	Unit
Number of Monte Carlo Trials	N_{trials}	10-30	
Carrier frequency	f_0	20.0	GHz
User baud rate	R_s	500.00	Msymb/s
Total payload RF power per carrier	P_T^c	2.0-4.0	kW
Min. ACM physical layer SNIR	$\text{SNIR}_{\min}$	-10.00	dB
User minimum spacing coefficient	$\rho_{\min}$	1.10	
Minimum satellite elevation angle	$\alpha_{\min}$	5.00	degrees
Array size	D_A	1.2-2.0	m
Array element aperture efficiency	η_E	-1	dB
Array elements normalized spacing	d_A/λ	1.4-2.6	
MB normalized beam spacing	S_{MB}^n	0.2-1.0	
Number of array elements	N_T	2025-9025	
Number of feeds/users ratio	N_T/N_U	1-6	
Number of simult. active users	N_U	405-1805	
Norm. MD-MIQP RRM min. dist.	$\rho_{\min}$	0.8-1.2	
Earth radius	R_E	6378	km
Orbit height	h_S	35780	km
User terminal antenna gain	G_R^U	41.45	dBi
User terminal antenna noise temp.	T_R^U	224.5	K

of users uniformly distributed (black points). Each user is assigned to a colour out of the ten available. Observing the distribution of users sharing the same colour, identifiable as a resource slice, it can be noticed that the user for each slice exhibit a minimum distancing. In the following statistical analysis of capacity, the users distributions will be generated per slice satisfying a minimum distancing by mean of the described Poisson circle distribution.

III. M-MIMO PERFORMANCE ANALYSIS

For assessing the M-MIMO performance we have been selecting a couple of reference configurations based on a geostationary (GEO) satellite with two different DRA sizes. The GEO orbit selection is arbitrary as the model provided is also applicable to other satellite orbits. However, techniques like MF, ZF and MMSE will be even more challenging to implement for non GEO case due to the the more link dynamic conditions. Table 1 summarizes the key system parameters adopted for the following numerical simulations. When a range of values is specified, it means that the sensitivity to this specific parameter has been optimized in the specified range.

The results reported in the following are organized in four main classes: medium and large array[9] size each subdivided in reduced and relaxed array element spacing. For each class we also consider two levels of RF power to assess its impact on the system performance. The two array size classes allow to understand the advantages of scaling the array physical size while keeping the same RF power. For each class, two sub-classes have been investigated i.e. reduced and relaxed array spacing. The reduced array spacing was selected to obtain a relatively high ratio for the number of array feeds versus the number of active users (e.g. ≥ 5) to comply with M-MIMO typical assumptions [1]. The relaxed spacing, still compliant with the need to keep the grating lobes outside the coverage area, was investigated to assess the performance impact of a reduction in the number of array elements. In this case, seeking for optimum performance, we have been reducing N_T/N_U down to 1 but eventually selecting 2 as the preferred value.

[9]Although full analysis and optimization of the large array has been performed, we only report the summary results to limit the section length.

1) MEDIUM SIZE ARRAY WITH REDUCED SPACING

In Sec. II-D we have been showing different approaches to normalize the precoding matrix norm. As a first step, we have been investigating the best solution considering the fact that the total satellite DRA RF power P_T^c is limited and the DRA array element power is also bounded by the individual HPAs maximum operating power in multi-carrier conditions $P_A^{\max}$ with $P_A^{\max} = P_T^c/N_T$. Simulation results are summarized in Table 2 for Shannon throughput and in Table 3 for DVB-S2X physical layer. It is apparent that the approach proposed by CTTC provides the best performance for all M-MIMO schemes. In particular, by ensuring that all DRA HPAs are driven at the same power level, we achieve the maximum use of the available RF power in particular for ZF and MMSE M-MIMO. Overall, the CTTC throughput improvement compared to the Taricccо's one is more than 200 % for ZF and MMSE and at least 230 % for MF/MB. For the modified Taricco normalization the CTTC improvement reduces to 9 % for MF/MB, 13 % for ZF and 16 % for MMSE. This means that the benefit resulting from the extra RF power made available by the CTTC normalization is superior to the reduction in co-channel interference mitigation allowed by the modified Taricco's approach. This finding holds true also for $P_T^c = 4$ kW. We also investigated the impact of removing the first step in the power normalization corresponding to an equal power allocation per user. It was found that removing this condition has no visible impact for MF, MB and MMSE techniques, while it is worsening the ZF performance.

Based on the above findings, the CTTC power normalization has been adopted for the rest of the paper being the best performer among all schemes.

As explained in Sec. II-G, in alternative to the uniform random user distribution we proposed a minimum distance algorithm to optimize the M-MIMO performance both in terms of throughput maximization and outage minimization. As first step, we optimized the normalized minimum distance (see Sec. II-G) and we found an optimum normalized distance value of $\rho_{\min} = 1.1$. This finding has been confirmed also for the case of 4 kW payload power and relaxed spacing. The impact of adopting the proposed MD-MIQP RRM approach is quite dramatic as shown in Table 4 and Table 5. The simulation results clearly indicate the major advantage of using the MD-MIQP RRM algorithm. For MF and MB the throughput increase is around 75 %, while for MMSE the improvement amounts to about 55 % being MMSE scheme more robust to the co-channel interference. For ZF the throughput advantage is about 170 %, but even more important, the related outage probability reduction from 29 to 0.24 %.

TABLE 2. Simulated M-MIMO Shannon throughput for a 1.2 × 1.2 m DRA as a function of the precoding matrix normalization algorithm: total RF power $P_T^c = 2$ kW, $R_s = 500$ Mbaud, $N_T/N_U = 5$, MD-MIQP RRM $\rho_{\min} = 1.1$, MB beams normalized spacing $S^n_{\text{MB}} = 0.2$.

M-MIMO technique	Throughput Shannon (Gbps) PC matrix norm. algorithm			Optimum DRA spacing d_A/λ
	Taricco	Mod. Taricco	CTTC	
MF	1.131e+02	3.548e+02	3.785e+02	1.6/1.6/1.6
MB	1.112e+02	3.485e+02	3.699e+02	1.6/1.6/1.6
ZF	1.080e+02	2.964e+02	3.339e+02	1.6/1.6/1.8
MMSE	1.125e+02	3.496e+02	4.047e+02	1.6/1.6/1.6

TABLE 3. Simulated M-MIMO DVB-S2X throughput for a 1.2 × 1.2 m DRA as a function of the precoding matrix normalization algorithm: total RF power $P_T^c = 2$ kW, $R_s = 500$ Mbaud, $N_T/N_U = 5$, MD-MIQP RRM $\rho_{\min} = 1.1$, MB beams normalized spacing $S^n_{\text{MB}} = 0.2$.

M-MIMO technique	Throughput DVB-S2X (Gbps) PC matrix norm. algorithm			Optimum DRA spacing d_A/λ
	Taricco	Mod. Taricco	CTTC	
MF	7.243e+01	2.737e+02	2.967e+02	1.8/1.6/1.6
MB	7.024e+01	2.713e+02	2.926e+02	1.6/1.6/1.6
ZF	6.708e+01	2.370e+02	2.809e+02	1.8/1.6/1.8
MMSE	7.197e+01	2.732e+02	3.189e+02	1.8/1.6/1.6

TABLE 4. Simulated M-MIMO Shannon throughput for a 1.2 × 1.2 m DRA as a function of the RRM algorithm: total RF power $P_T^c = 2$ kW, $R_s = 500$ Mbaud, $N_T/N_U = 5$, MB beams normalized spacing $S^n_{\text{MB}} = 0.2$.

M-MIMO technique	Throughput Shannon (Gbps) RRM algorithm		Optimum DRA spacing d_A/λ
	Random	Min distance	
MF	2.158e+02	3.783e+02	1.6
MB	2.129e+02	3.699e+02	1.6
ZF	1.221e+02	3.339e+02	1.8
MMSE	2.597e+02	4.047e+02	1.6

TABLE 5. Simulated M-MIMO DVB-S2X throughput for a 1.2 × 1.2 m DRA as a function of the RRM algorithm: total RF power $P_T^c = 2$ kW, $R_s = 500$ Mbaud, $N_T/N_U = 5$, MB beams normalized spacing $S^n_{\text{MB}} = 0.2$.

M-MIMO technique	Throughput DVB-S2X (Gbps) RRM algorithm		Optimum DRA spacing d_A/λ
	Random	Min distance	
MF	1.611e+02	2.967e+02	1.6
MB	1.585e+02	2.926e+02	1.6
ZF	9.321e+01	2.809e+02	1.8
MMSE	2.006e+02	3.189e+02	1.6

The MB normalized spacing $S^n_{\text{MB}} = 0.2$ adopted in the simulations is based on an interesting result presented in Fig. 12, where the throughput of the different M-MIMO solutions is compared to the MB one when modifying the

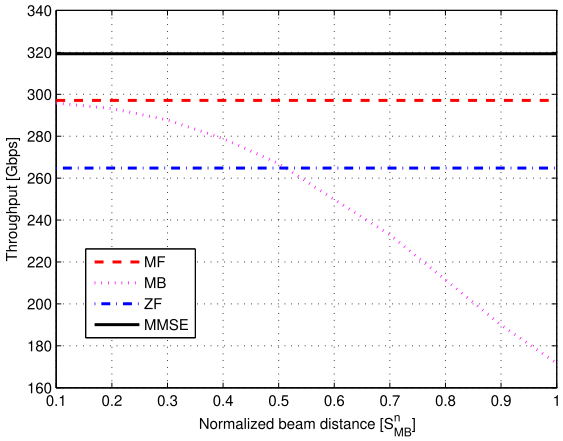

FIGURE 12. Simulated M-MIMO DVB-S2X throughput for a 1.2 × 1.2 m DRA as a function of the MB beam normalized beam spacing S^n_{MB}: $P_T^c = 2000$ W, $R_s = 500$ Mbaud, $N_T/N_U = 5$, minimum distance RRM, $d_A/\lambda = 1.6$.

normalized beam spacing. It is apparent that, by decreasing the fixed beam normalized spacing S^n_{MB}, the performance difference between the MB and the MF is vanishing. This is because the grid of fixed beams becomes so fine that it allows to select the beam that is maximizing the gain towards all users location as the MF does. It is important to remark that, as elaborated in Sec. VI, the MB is simply realized through a fixed beam pattern with an input switch to connect the users to be served and any instant without any need for user physical channel estimation except for a raw position knowledge. This means that, when accounting conventional M-MIMO performance with channel estimation errors, the MB performance will be even superior than the more complex solutions requiring channel feedback.

This results is in contrast to the Viasat patent finding reported in [36], where it is shown that with full frequency reuse the optimum beam overlap is for a cross-over point of −6 dB or more, i.e. for fairly separated beams. This finding seems related to the system model adopted. In particular, the assumption of a fixed E_s/N_0 value which has an impact on the sensitivity analysis. Our approach is considered more realistic as we fix the antenna size and the *total* RF power and deriving the available E_s/N_0 as a function of the DRA key parameters.

Finally, it is interesting to remark the limited performance loss provided by the MB solution considering that, by exploiting a fixed grid of beams, does not require any users' channel feedback and complex on-board computations like is the case for MMSE, ZF and to a less extent for MF. More details about the practical MB implementation aspects can be found in Sec. VI.

For the medium size array case characterized by a squared shape with length $D_A = 1.2$ m, we have been first optimizing the array element spacing d_A/λ and then the ratio between the number of array elements and active users N_T/N_U. Looking at the results for $N_T/N_U = 5$ reported in Fig. 13, it is apparent

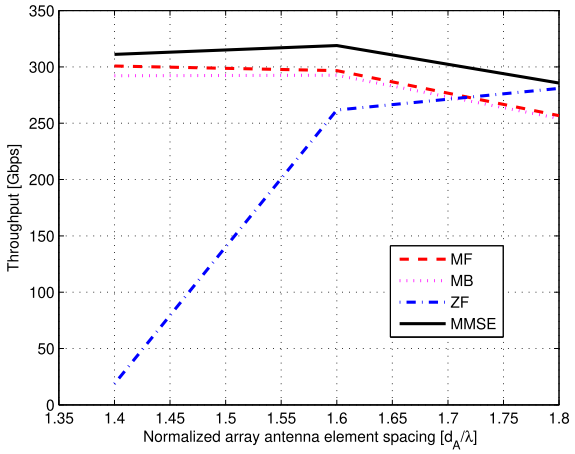

FIGURE 13. Simulated M-MIMO DVB-S2X throughput for a 1.2 × 1.2 m DRA as a function of the array element spacing d_A/λ: $P_T^c = 2000$ W, $R_S = 500$ Mbaud, $N_T/N_U = 5$, MD-MIQP RRM $\rho_{\min} = 1.1$, MB beams normalized spacing $S_{MB}^n = 0.2$.

that for MB, MF and MMSE the throughput is optimized for $d_A/\lambda = 1.6$. Instead, for ZF the throughput is maximized for $N_T/N_U = 5$ and $d_A/\lambda = 1.8$. This is because the ZF outage is not zero until $d_A/\lambda = 1.6$.

We have also analyzed the throughput dependency on the active antenna RF power P_T^c. The corresponding simulation results are summarized in Table 6 and Table 7 for the Shannon and DVB-S2X cases, respectively. It appears that by doubling P_T^c from 2 kW to 4 kW with fixed bandwidth, MF and MB techniques increase the throughput by 33 %, while ZF and MMSE by 52 % for Shannon and about the same in case of DVB-S2X. Instead, doubling the bandwidth and the power will provide a 100 % throughput increase. Consequently,

TABLE 6. Simulated M-MIMO Shannon throughput for a 1.2 × 1.2 m DRA as a function of the total RF power: $R_S = 500$ Mbaud, $N_T/N_U = 5$, MD-MIQP RRM $\rho_{\min} = 1.1$, MB beams normalized spacing $S_{MB}^n = 0.2$.

M-MIMO technique	Throughput Shannon (Gbps) DRA total RF power P_T^c (W) 2000	4000	Optimum DRA spacing d_A/λ
MF	3.783e+02	5.050e+02	1.6
MB	3.699e+02	4.922e+02	1.6
ZF	3.339e+02	5.079e+02	1.8
MMSE	4.047e+02	5.697e+02	1.6

TABLE 7. Simulated M-MIMO DVB-S2X throughput for a 1.2 × 1.2 m DRA as a function of the total RF power: $R_S = 500$ Mbaud, $N_T/N_U = 5$, MD-MIQP RRM $\rho_{\min} = 1.1$, MB beams normalized spacing $S_{MB}^n = 0.2$.

M-MIMO technique	Throughput DVB-S2X (Gbps) DRA total RF power P_T^c (W) 2000	4000	Optimum DRA spacing d_A/λ
MF	2.967e+02	4.012e+02	1.6
MB	2.926e+02	3.895e+02	1.6
ZF	2.809e+02	4.262e+02	1.8
MMSE	3.189e+02	4.629e+02	1.6

the latter solution is preferable considering that in Ka-band the bandwidth available is up to 2.5 GHz.

2) MEDIUM SIZE ARRAY WITH RELAXED SPACING

As explained before, we also explored a relaxation of the beam spacing to reduce the DRA complexity in terms of RF chains and radiating elements for the same physical array size. Looking at Fig. 14-(a) it appears that for $N_T/N_U = 5$ there is a marked monotonic reduction in the throughput increasing the array spacing. Instead, by reducing N_T/N_U to 2, as shown in Fig. 14-(b), the previously observed throughput loss is almost completely recovered. This approach corresponds to keep constant the number of array elements N_T independently from the adopted spacing. However, lowering further the N_T/N_U ratio down to 1 reduces the throughput. This means that moving from $d_A/\lambda = 1.6$ to $d_A/\lambda = 2.4$ we can reduce the number of array elements and RF chains from 2500 to 1156 (a factor 2.16) with a M-MIMO throughput reduction of only 3 %. This result is counter-intuitive as it seems to violate one key M-MIMO assumption but a similar indication was highlighted in terrestrial M-MIMO findings reported in [14]. This aspect will be clarified in Sec. III-A.

TABLE 8. Optimized MB pragmatic M-MIMO parameters.

Parameter	Symbol	Value
RRM User minimum spacing coefficient	$\rho_{\min}$	1.10
Array elements normalized spacing	d_A/λ	2.4
MB normalized beam spacing	S_{MB}^n	0.2
Number of array elements for 1.2 m array	N_T	1156
Number of array elements for 2.0 m array	N_T	3136
Number of active users for 1.2 m array	N_U	482
Number of active users for 2.0 m array	N_U	1568
Number of feeds/users ratio	N_T/N_U	2
Precoding matrix normalization		CTTC

A. PRAGMATIC M-MIMO NUMERICAL RESULTS SUMMARY AND CONSIDERATIONS

The best parameters derived for pragmatic M-MIMO implementation with relaxed feed spacing are summarized in Table 8. The simulated throughput summary exploiting the optimized configurations is reported in Tables 9 and 10 for the Shannon and DVB-S2X cases. We observe that the throughput is almost growing with the square of the array dimension D_A i.e. proportional to the array area. Instead, as observed before, the throughput shows a logarithmic dependency on the RF power. The optimized MB MD-MIQP RRM M-MIMO performance is closely following the MF performance. Instead, the ZF algorithm performance is penalised by the selected configuration. This is because for this array element spacing, the ZF throughput is heavily affected by the high outage probability. MMSE results, although slightly better than MB, are assuming perfect channel estimation that, as previously discussed, is not achievable in practice.

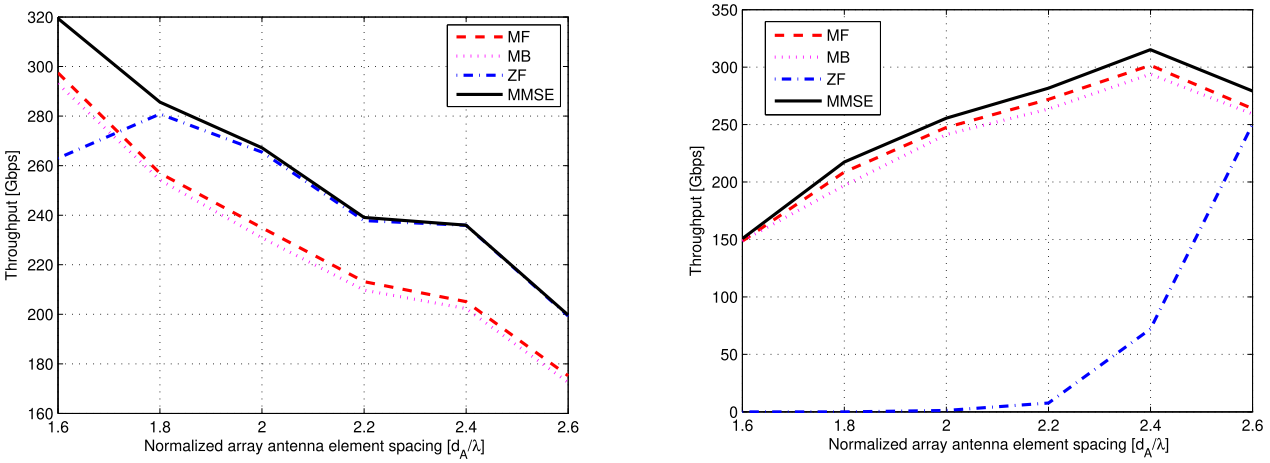

(a) $N_T/N_U = 5$ (b) $N_T/N_U = 2$

FIGURE 14. Simulated M-MIMO DVB-S2X throughput for a 1.2 × 1.2 m DRA as a function of the array element spacing d_A/λ: $P_T^c = 2000$ W, $R_s = 500$ Mbaud, $N_T/N_U = 2,\ 5$, MD-MIQP RRM $\rho_{\min} = 1.1$, MB beams normalized spacing $S_{MB}^n = 0.2$.

TABLE 9. M-MIMO Shannon throughput results.

Configuration			Throughput Shannon (Gbps)			
R_s (Mbaud)	D_A (m)	P_T^c (kW)	MB	MF	ZF	MMSE
500	1.2	2	3.60E+02	3.69E+02	1.00E+02	3.89E+02
500	1.2	4	4.80E+02	4.93E+02	1.55E+02	5.39E+02
500	2.0	2	9.57E+02	9.81E+02	6.57E+01	1.02E+03
500	2.0	4	1.26E+03	1.29E+03	9.28E+01	1.39E+03

TABLE 10. M-MIMO DVB-S2X throughput results.

Configuration			Throughput DVB-S2X (Gbps)			
R_s (Mbaud)	D_A (m)	P_T^c (kW)	MB	MF	ZF	MMSE
500	1.2	2	2.93E+02	3.01E+02	7.49E+01	3.15E+02
500	1.2	4	3.74E+02	3.83E+02	1.18E+02	4.22E+02
500	2.0	2	7.78E+02	8.00E+02	4.72E+01	8.35E+02
500	2.0	4	9.85E+02	1.01E+03	6.88E+01	1.08E+03

We now introduce the overall normalized payload system efficiency defined as

$$\eta_P = \frac{T}{R_s P_{\mathrm{T}}^c D_A^2} \quad [\mathrm{Mbps/(MBaud \cdot W \cdot m^2)}]. \tag{67}$$

The η_P figure of merit allows to account for normalized throughput in terms of occupied user bandwidth, payload RF power and DRA antenna area. Utilizing (67) we have been deriving the normalized payload efficiency for the M-MIMO configurations previously analyzed. The corresponding results are reported in Table 11 and Table 12 for the Shannon and DVB-S2X cases. It is interesting to remark that the best normalized payload system efficiency results are obtained for $P_T^c = 2$ kW. The payload system efficiency improvement is maintained also by further reducing P_T^c. However, by doing so, at a certain point we start to impact the link availability. This is because in certain locations we may reach the minimum SNIR supported by the air interface.

TABLE 11. M-MIMO Shannon normalized payload efficiency results.

Configuration			Payload efficiency Shannon (Mbps/(Mbaud·W/m^2))			
R_s (Mbaud)	D_A (m)	P_T^c (kW)	MB	MF	ZF	MMSE
500	1.2	2	2.50E-01	2.57E-01	6.97E-02	2.70E-01
500	1.2	4	1.67E-01	1.71E-01	5.39E-02	1.87E-01
500	2.0	2	2.39E-01	2.45E-01	1.64E-02	2.56E-01
500	2.0	4	1.57E-01	1.62E-01	1.16E-02	1.74E-01

TABLE 12. M-MIMO DVB-S2X normalized payload efficiency results.

Configuration			Payload efficiency Shannon (Mbps/(Mbaud·W/m^2))			
R_s (Mbaud)	D_A (m)	P_T^c (kW)	MB	MF	ZF	MMSE
500	1.2	2	2.04E-01	2.09E-01	5.20E-02	2.19E-01
500	1.2	4	1.30E-01	1.33E-01	4.11E-02	1.47E-01
500	2.0	2	1.94E-01	2.00E-01	1.18E-02	2.09E-01
500	2.0	4	1.23E-01	1.26E-01	8.61E-03	1.35E-01

Instead, η_P slightly degrades passing from $D_A = 2$ m to 4 m. Clearly the absolute throughput improves almost proportionally to the DRA surface.

At this point, we provide a critical review of the previous satellite M-MIMO analysis key findings taking into account terrestrial M-MIMO myths considerations reported in [14].

More specifically:

1) M-MIMO works also in line-of-sight conditions (see Myth 2 in [14]).
2) M-MIMO performance can be achieved by open loop beam-forming techniques (see Myth 3 in [14]).
3) M-MIMO performance loss by linear processing is modest (see Myth 5 in [14]).
4) M-MIMO does not require an order of magnitude more antennas than users (see Myth 6 in [14]).

Point 1) was one of the assumptions taken at the beginning of this work supported by M-MIMO literature review. We can also consider that the Myth 2 discussion in [14], aiming at removing the worst-case users affecting the system performance in a non favourable propagation environment (i.e. not providing users' orthogonality), is achieved by the MD-MIQP RRM algorithm proposed. Point 2) is implemented by means of the MB M-MIMO solution whereby the users are assigned to the pre-formed beams providing the highest gain. Differently from what discussed in [14] for terrestrial systems, in our case the approach is scalable, as the beam is selected solely based on the approximate user's geographical location which requires very limited signalling information. Point 3) has not been investigated in this work. However, work related to the downlink of multi-beam satellite [37], has shown marginal gains adopting MMSE-SIC techniques compared to more conventional frequency reuse solutions. Point 4) has been confirmed by our findings showing that the ratio between number of antenna elements and active users around 2 achieves quasi optimum results. This ratio is well below the typical order of magnitude normally assumed for M-MIMO.

IV. CONVENTIONAL FREQUENCY REUSE SCHEME PERFORMANCE ANALYSIS

This section is providing performance results of a more conventional active payload antenna with the same key parameters as the one used for M-MIMO. This approach allows a fair comparison of the M-MIMO advantages. Conventional CFR schemes, described in Sec. II-F, are partitioning the available user link bandwidth R_s^{TOT} in N_c colours. This solution has two main advantages compared to M-MIMO full frequency reuse: a) reducing the other beams co-channel interference; b) reducing the required feeder link bandwidth. Intuitively, the consequent reduced beam user link bandwidth R_s^{TOT}/N_c compared to M-MIMO R_s^{TOT}, is expected to provide a lower system throughput.

A. CONVENTIONAL FREQUENCY REUSE SYSTEM PARAMETERS

For generating the conventional frequency reuse reference system performance we have been selecting a couple of GEO satellite antenna configurations similar to the M-MIMO ones. Table 13 summarizes the key system parameters adopted for the following numerical simulations. As before, when a range of values is specified, it means that the sensitivity to this specific parameter has been optimized in the specified range. The number of colours is fixed to 4 as attempts to use 2 or 3 colours provided sub-optimum performance.

It should be remarked that is normal practice to separate the beams by a normalized distance S_{MB}^n equal to 1 corresponding to a beam cross-over of $-$ 4 dB (see for example ACM results for 4CFR reported in [36] also showing a very mild dependency on the beam spacing). Instead, we will show, that to boost DRA performance the normalized beam spacing shall be considerably reduced.

TABLE 13. Simulation system parameters.

Parameter	Symbol	Value	Unit
Number of Monte Carlo Trials	N_{trials}	50	
Carrier frequency	f_0	20.0	GHz
Total baud rate	R_s^{TOT}	500.00	Msymb/s
Number of colors	N_c	4	
Number of polarization	N_p	1	
User baud rate	R_s	125.00	Msymb/s
Total payload RF power	P_T^c	2.0-4.0	kW
Min. ACM physical layer SNIR	$\mathrm{SNIR}_{\mathrm{min}}$	-10.00	dB
Min. satellite elevation angle	α_{min}	5.00	degrees
Array size	D_A	1.2-2.0	m
Array element aperture efficiency	η_E	-1	dB
Array elements normalized spacing	d_A/λ	1.4-4.0	
MB normalized beam spacing	S_{MB}^n	0.3-1.0	
Number of array elements	N_T	3328-12544	
Number of beams/users ratio	N_B/N_U	1-4	
Number of simult. active users	N_U	405-1805	
Earth radius	R_E	6378	km
Orbit height	h_S	35780	km
User terminal antenna gain	G_R^U	41.45	dBi
User terminal antenna noise temp.	T_R^U	224.5	K

B. CFR NUMERICAL RESULTS

1) MEDIUM SIZE ARRAY WITH REDUCED SPACING

We first assessed the conventional 4 colour frequency reuse scheme with the medium size 1.2 m DRA using the 2 kW RF power assumption. Looking at the results reported in Fig. 15, it is interesting to observe that for $d_A/\lambda = 1.6$ (but the same finding apply to $d_A/\lambda = 1.4$), the throughput performance are highly dependent on the normalized beam spacing. The best result is obtained for $S_{MB}^n = 0.5$. This means that also in a conventional 4 colour frequency reuse scheme a quite large overlap among beams is preferable. This approach creates a larger co-channel interference contribution but increases the amount of simultaneous active beams, hence served users, overall increasing the aggregated throughput up to $S_{MB}^n = 0.5$. Beyond this value the interference increase is not counterbalanced by the number of active beams increase. It should be remarked that this beam spacing approach is non conventional as typical multi-beam antenna design assumes a normalized spacing $S_{MB}^n = 1$.

Instead the DRA dependency on the radiating element spacing resulted to be weak (see Fig. 16). For consistency with M-MIMO results we for the reduced array spacing we have been using the slightly sub-optimum value of $d_A/\lambda = 1.6$.

2) MEDIUM SIZE ARRAY WITH RELAXED SPACING

Similarly to what was done for the M-MIMO case, we have investigated the impact of a relaxation of the DRA feed elements distance to reduce the DRA complexity. The simulation results for a medium size array are summarized in Fig. 17. It is evident that for CFR with beam spacing $S_{MB}^n = 0.5$ the throughput dependency to the array feeds spacing is mild up to $d_A/\lambda = 2.4$ for which value there is a secondary throughput peak. To this secondary peak corresponds a 1.2%

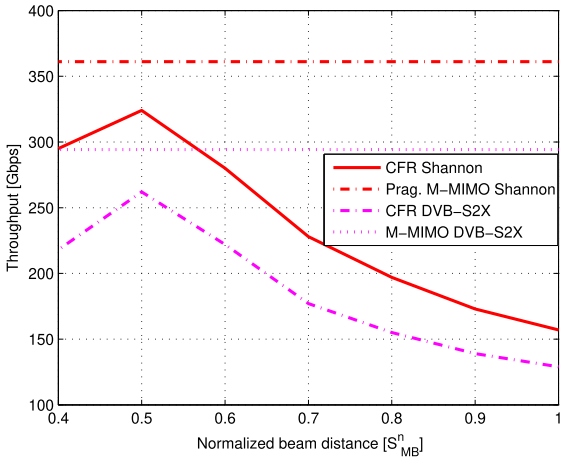

FIGURE 15. Simulated 4 colours throughput for a 1.2 × 1.2 m DRA as a function of the normalized beam spacing S^n_{MB}: $P^c_T = 2000$ W, $R_S = 125$ Mbaud, $N_B/N_U = 1$, array element spacing $d_A/\lambda = 1.6$.

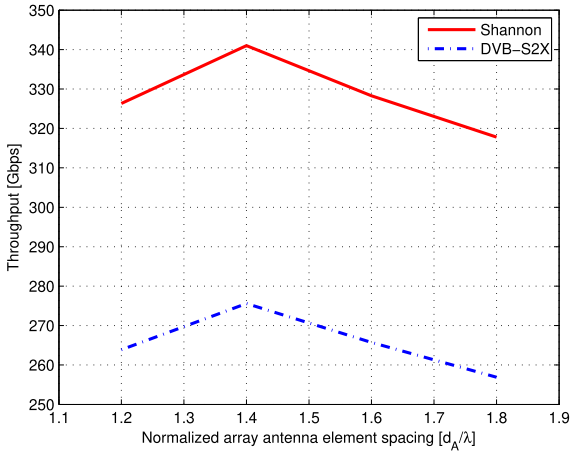

FIGURE 16. Simulated 4 colours throughput for a 1.2 × 1.2 m DRA as a function of the array element spacing: $P^c_T = 2000$ W, $R_S = 125$ Mbaud, $N_B/N_U = 1$, MB beams normalized spacing $S^n_{MB} = 0.5$.

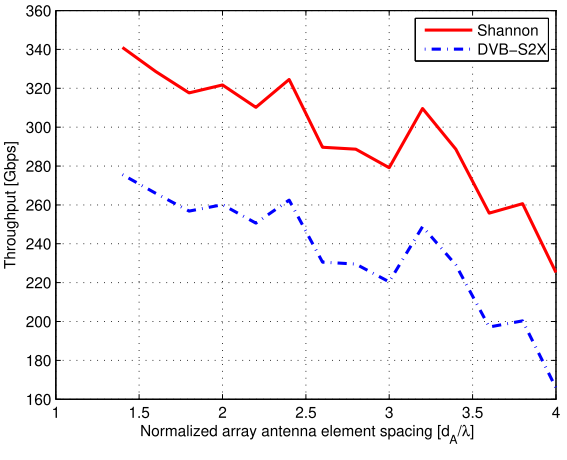

FIGURE 17. Simulated 4 colours throughput for a 1.2 × 1.2 DRA as a function of the narrow array element spacing: $P^c_T = 2000$ W, $R_S = 125$ Mbaud, $N_B/N_U = 1$, MB beams normalized spacing $S^n_{MB} = 0.5$.

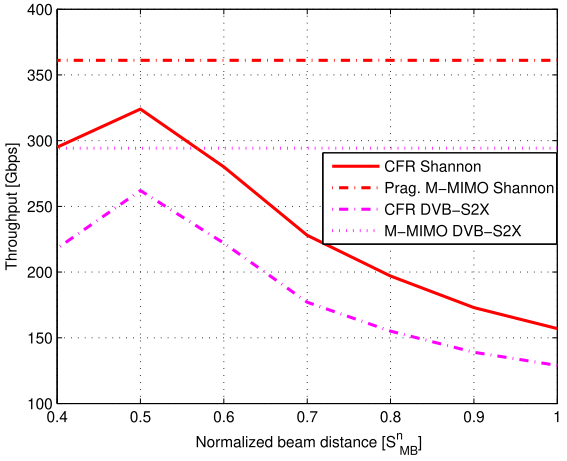

FIGURE 18. Simulated 4 colours throughput for a 1.2 × 1.2 m DRA as a function of the relaxed normalized spacing S^n_{MB}: $P^c_T = 2000$, $R_S = 125$ Mbaud, $N_B/N_U = 1$, array element spacing $d_A/\lambda = 2.4$.

throughput drop compared to $d_A/\lambda = 1.6$. As remarked in Sec. III-2, this spacing allows to achieve a substantial reduction in terms of array elements (factor 2.16) with a throughput reduction limited to few percent. The throughput dependency on the beam spacing is reported in Fig. 18. It is apparent that the typical spacing adopted in DRA corresponding to $d_A/\lambda = 3.6$ provides sub-optimum results i.e a throughput reduction of 11% compared to $d_A/\lambda = 2.4$. Additional simulations results reported in Fig. 18, confirmed the optimum value $S^n_{MB} = 0.5$ previously found for the case of reduced array spacing.

C. SUMMARY COMPARISON OF CFR VS M-MIMO RESULTS

In the following we provide a summary comparison of throughput performance for the optimized M-MIMO and 4CFR / 4CFR^{++} configurations for the medium and large array cases.

1) MEDIUM ARRAY

The medium array M-MIMO and CFR comparison is reported in Tables 14 and 15 for the Shannon and DVB-S2X cases respectively. It is apparent that the great performance improvement (i.e. a throughput doubling) provided by 4CFR^{++} over 4CFR. The M-MIMO MB adds some extra performance boost compared to 4CFR^{++}. It should be recalled that while the pragmatic MB-MIMO and 4CFR / 4CFR^{++} performance are achievable in practice, MMSE M-MIMO represents a theoretical upper bound as it will require perfect channel estimation and complex on-board processing. The MMSE throughput advantage compared to 4CFR and M-MIMO-MB increases with the payload power because of its capability to better cope with the co-channel interference. However, for a realistic RF power $P^c_T = 2$ kW assumption, the M-MIMO-MB loss wrt to ideal MMSE is only 9 %.

TABLE 14. Throughput comparison 4CFR vs M-MIMO with Shannon for a 1.2 × 1.2 m DRA with optimized narrow feed spacing.

Technique	Throughput Shannon (Gbps) DRA total RF power P_T^c (W) 2000	4000	Relative throughput performance % vs 4CFR	4CFR^{++}
4CFR	1.573e+02	1.978e+02	0 / 0	
4CFR^{++}	3.243e+02	4.284e+02	106.1 / 116.6	0 / 0
M-MIMO-MB	3.611e+02	4.798e+02	129.5 / 142.6	11.3 / 12.0
M-MIMO MMSE	3.888e+02	5.394e+02	147.1 / 172.7	19.9 / 25.9

TABLE 15. Throughput comparison 4CFR vs M-MIMO with DVB-S2X for a 1.2 × 1.2 m DRA with optimized relaxed feed spacing ($D/\lambda = 2.4$).

Technique	Throughput DVB-S2X (Gbps) DRA total RF power P_T^c (W) 2000	4000	Relative throughput performance % vs 4CFR	4CFR^{++}
4CFR	1.285e+02	1.642e+02	0 / 0	
4CFR^{++}	2.623e+02	3.369e+02	104.1 / 105.2	0 / 0
M-MIMO-MB	2.942e+02	3.739e+02	129.0 / 127.7	11.0 / 11.0
M-MIMO MMSE	3.154e+02	4.224e+02	145.4 / 157.3	20.2 / 25.4

2) LARGE ARRAY

The medium array M-MIMO and CFR comparison is reported in Tables 16 and 17 for the Shannon and DVB-S2X cases respectively. The same considerations reported for the medium array case are also applicable here.

TABLE 16. Throughput comparison 4CFR vs M-MIMO with Shannon for a 2.0 × 2.0 m DRA with relaxed feed spacing ($D/\lambda = 2.4$).

Technique	Throughput Shannon (Gbps) DRA total RF power P_T^c (W) 2000	4000	Relative throughput performance % vs 4CFR	4CFR^{++}
4CFR	4.249e+02	5.491e+02	0 / 0	
4CFR^{++}	8.706e+02	1.182e+03	104.9 / 115.2	0 / 0
M-MIMO-MB	9.572e+02	1.259e+03	125.2 / 129.4	10.0 / 6.6
M-MIMO MMSE	1.024e+03	1.395e+03	140.9 / 154.	17.6 / 17.6

TABLE 17. Throughput comparison 4CFR vs M-MIMO with DVB-S2X for a 2.0 × 2.0 m DRA with relaxed feed spacing ($D/\lambda = 2.4$).

Technique	Throughput DVB-S2X (Gbps) DRA total RF power P_T^c (W) 2000	4000	Relative throughput performance % vs 4CFR	4CFR^{++}
4CFR	3.472e+02	4.560e+02	0 / 0	
4CFR^{++}	7.039e+02	9.305e+02	102.7 / 104.1	0 / 0
M-MIMO-MB	7.777e+02	9.850e+02	124.0 / 116.0	9.9 / 5.9
M-MIMO MMSE	8.352e+02	1.083e+03	140.5 / 137.6	18.7 / 16.1

V. OVERALL RESULTS SUMMARY

The summary of the throughput simulated exploiting the optimized configurations are reported in Tables 18 and 19 for the Shannon and DVB-S2X cases. We observe that the throughput is almost growing with the square of the array dimension D_A. Instead, as observed before, the throughput shows a logarithmic dependency on the RF power. We also remark that the MB M-MIMO approach closely follows the MF performance. The ZF algorithm performance is instead penalised for the selected DRA configuration, as for the selected array spacing it is affected by heavy outage probability, thus not usable in practice. MMSE results, although slightly better, are obtained assuming perfect channel estimation. In practice, even assuming that the MMSE matrix inversion is implementable, channel estimation errors and other implementation aspects in a satellite systems will make this scheme less appealing than the MB M-MIMO. MB M-MIMO is also highly attractive for non GEO orbits where the constellation dynamics will make solutions based on channel estimate even less attractive.

The normalized payload efficiency results are reported in Table 20 and Table 21 for the Shannon and DVB-S2X cases. It is interesting to remark that the best results are obtained for $P_T^c = 2$ kW while η_P slightly degrades passing from $D_A = 2$ m to 4 m. Clearly the absolute throughput improves increasing the DRA size.

VI. A PRAGMATIC M-MIMO PAYLOAD DESIGN

The central stage of the payload is the bulk beamforming stage constituted by a bi-dimensional fixed beam beamforming (FB-BFN) matrix realizing the high-density fixed beam lattice. A beam selecting matrix (BSM) allows to select and address the active out of the full number of available ones generated by the fixed beam beamforming matrix. A high level block diagram is reported in Fig. 19.

Details of the beamforming stage of the payload are shown in Fig. 20.

The FB-BFN matrix should generate a pre-defined set of N_B beams with beam centers corresponding to the points of the lattice $\Lambda(S_{\mathrm{MB}})$ within the disk of radius $\sin(\vartheta_{\max})$ in the u, v space. Efficient techniques of beamforming pose additional constraints on the number of input ports and number of output ports corresponding to real or fictitious array elements. For this reason the FB-BFN matrix is shown to be oversized with a number of input ports N_{FB} and a number of output ports N_{FT}. Of the N_{FT} output logic ports, N_T correspond to physical radiating elements. If the beamforming is performed in the digital domain, this N_T ports must be physically implemented with corresponding Digital-to-Analogue mixed signal converters. Similarly to the total number of input ports N_{FB} of the fixed-beam beamforming matrix, some of the input corresponds to beams with steering directions outside the desired region-of-interest and do not need to be interconnected to previous stages. The BSM has a number of inputs equal to the number of instantaneous active users N_U and need to access the useful N_B ports of the fixed-beam beamforming matrix. While a general non-blocking architecture would be suitable, complexity reduction of the number of nodes of the beam selecting matrix can be obtained considering that some switching flexibility is realised by the previous

TABLE 18. CFR and M-MIMO Shannon throughput results.

Configuration			Throughput Shannon (Gbps)				
R_s (Mbaud)	D_A (m)	P_T^c (kW)	CFR^{++}	MB	MF	ZF	MMSE
500	1.2	2	3.24E+02	3.60E+02	3.69E+02	1.00E+02	3.89E+02
500	1.2	4	4.28E+02	4.80E+02	4.93E+02	1.55E+02	5.39E+02
500	2.0	2	8.71E+02	9.57E+02	9.81E+02	6.57E+01	1.02E+03
500	2.0	4	1.18E+03	1.26E+03	1.29E+03	9.28E+01	1.39E+03

TABLE 19. CFR and M-MIMO DVB-S2X throughput results.

Configuration			Throughput DVB-S2X (Gbps)				
R_s (Mbaud)	D_A (m)	P_T^c (kW)	CFR^{++}	MB	MF	ZF	MMSE
500	1.2	2	2.62E+02	2.93E+02	3.01E+02	7.49E+01	3.15E+02
500	1.2	4	3.37E+02	3.74E+02	3.83E+02	1.18E+02	4.22E+02
500	2.0	2	7.04E+02	7.78E+02	8.00E+02	4.72E+01	8.35E+02
500	2.0	4	9.31E+02	9.85E+02	1.01E+03	6.88E+01	1.08E+03

TABLE 20. CFR and M-MIMO Shannon normalized payload efficiency results.

Configuration			Payload efficiency Shannon (Mbps/(Mbaud·W/m^2))				
R_s (Mbaud)	D_A (m)	P_T^c (kW)	CFR^{++}	MB	MF	ZF	MMSE
500	1.2	2	2.25E-01	2.50E-01	2.57E-01	6.97E-02	2.70E-01
500	1.2	4	1.49E-01	1.67E-01	1.71E-01	5.39E-02	1.87E-01
500	2.0	2	2.18E-01	2.39E-01	2.45E-01	1.64E-02	2.56E-01
500	2.0	4	1.48E-01	1.57E-01	1.62E-01	1.16E-02	1.74E-01

TABLE 21. CFR and M-MIMO DVB-S2X normalized payload efficiency results.

Configuration			Payload efficiency DVB-S2X (Mbps/(Mbaud·W/m^2))				
R_s (Mbaud)	D_A (m)	P_T^c (kW)	CFR^{++}	MB	MF	ZF	MMSE
500	1.2	2	1.82E-01	2.04E-01	2.09E-01	5.20E-02	2.19E-01
500	1.2	4	1.17E-01	1.30E-01	1.33E-01	4.11E-02	1.47E-01
500	2.0	2	1.76E-01	1.94E-01	2.00E-01	1.18E-02	2.09E-01
500	2.0	4	1.16E-01	1.23E-01	1.26E-01	8.61E-03	1.35E-01

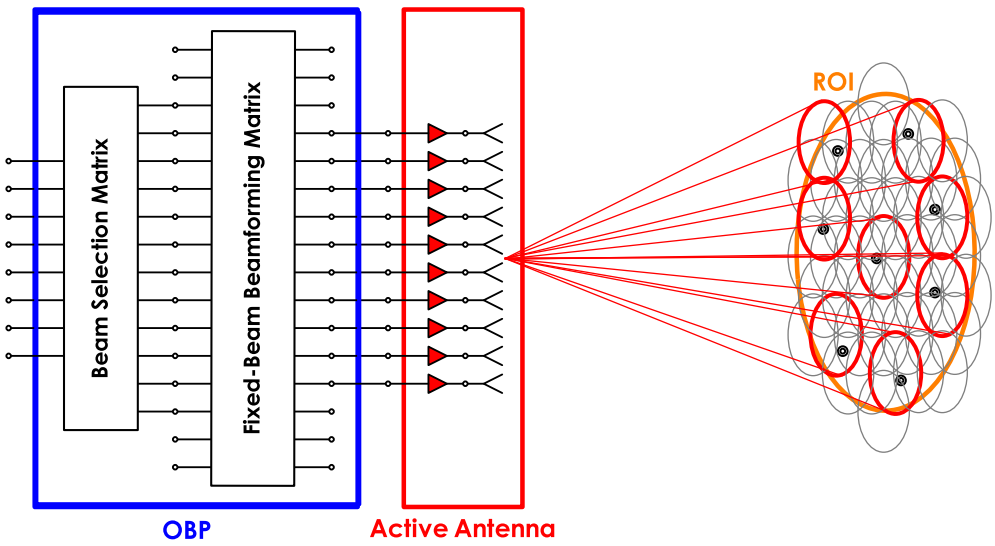

FIGURE 19. High level block diagram of the pragmatic M-MIMO payload.

TABLE 22. Proposed on-board processor architecture complex multiplications saving for MB and CFR++ techniques.

M-MIMO technique	Complex multiplications saving %			
	$D_A = 1.2$ m		$D_A = 2$ m	
	$d_A/\lambda = 1.6$ $N_T/N_U = 5$	$d_A/\lambda = 2.4$ $N_T/N_U = 2$	$d_A/\lambda = 1.6$ $N_T/N_U = 5$	$d_A/\lambda = 2.4$ $N_T/N_U = 2$
MB ($S^n_{MB} = 0.2$)	20.3	35.9	68.4	73.2
CFR++ ($S^n_{MB} = 0.5$)	97.5	97.7	99.0	99.2

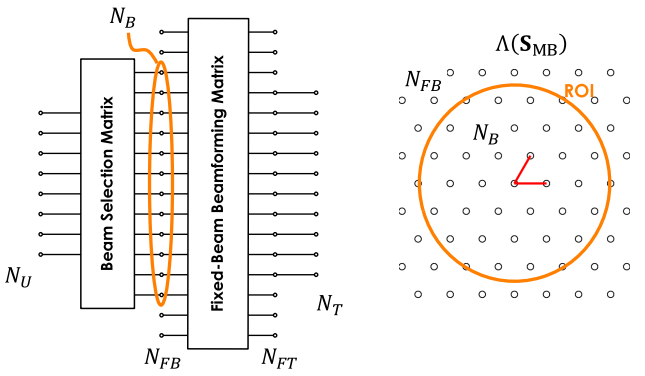

FIGURE 20. Details of the pragmatic M-MIMO payload.

stages of the payload or in the mapping of the feeder-link uplink with the accessible inputs of the beam selecting matrix.

Concerning the fixed-beam beamforming matrix, it can be realised by mean of efficient multistage networks which exploit the "divide and conquer" paradigm for solving large problems partitioning them in a set of smaller sub-problems easier to solve. An example of multistage networks is Fast Fourier Transform (FFT), which is complexity reduced technique to implement the Discrete Fourier Transform (DFT). It can be applied to periodic 1D lattices of radiating elements and periodic 1D lattices of fan-beams. Stacks of orthogonal 1D-FFTs can be employed in beamforming networks for planar phased array with placement both of the radiating elements and of the beams in a rectangular arrangement. For non rectangular placement of the radiating elements and/or beams, more complex theoretical frameworks must be recalled as those relevant to the Multi-Dimensional FFT (MD-FFT) [30]. Techniques based on MD-FFTs for planar lattices are particularly well suited for periodic arrays and have been implemented, tested and validated in a real-time proof-of-concept demonstrator [38] for arrays with number of beams to be generated equal to the number of antenna elements. In the present case, the high overlapping of the beams requires an oversizing of the MD-FFT and FFT input pruning, zero padding or Reconfigurable-MD-FFT architectures [42] can offer further advantages in terms of complexity reduction when there is a large unbalance in the numbers N_B, N_{FB}, N_{FT} and N_T.

To appreciate the advantages in complexity reduction of a multistage fixed-beam beamforming matrix based on a multi-stage MD-FFT we have to compare it with the multiplicative complexity of a standard reconfigurable beamforming network generating N_U beams with N_T antenna elements which would typically require $N_U N_T$ complex multiplications. The complexity of such a network would make it impractical due to the associated power consumption. Instead, the multiplicative complexity of a multistage MD-FFT goes with $N \log_2(N)$, where N is at the worst the maximum between N_{FB} and N_{FT}. Depending on the amount of beam overlap, the proposed approach can provide a multiplicative complexity reduction factor from 4 to 100. Furthermore, while a standard reconfigurable BFN must rely on general purpose non optimised complex multipliers, the arithmetic operators of the MD-FFT can be thoroughly optimised. Table 22 provides more specific results in terms of the percentage of complex multiplications reduction for MB and CFR++ techniques applying the proposed payload architecture. We observe that the gain is particularly large (factor 100) for CFR++ with large DRA size. The gain is less pronounced for the MB case (factor 3.7 max).

Finally it is worth mentioning that Fig. 19 and Fig. 20 refer to the simplified architecture for a single frequency slot. In case of use of multiple frequency slots, an equivalent number of parallel architectures (physical or logical) can work contemporarily and can be frequency multiplexed at element level.

VII. SUMMARY AND CONCLUSIONS

In this work we have been investigating a pragmatic approach to apply M-MIMO techniques to satellite broadband telecommunication systems. The resulting system throughput performances have been compared the achievable performance with the ultimate theoretical M-MIMO performance requiring complex on-board processing and cumbersome, not scalable user link channel state estimation. The proposed MB MIQDP-RRM M-MIMO design allows to approach the M-MIMO performance with affordable system and payload complexity without requiring users feedback except for a raw estimate of their geographical location. To achieve this result the following specific techniques have been developed:

- Novel RRM technique for M-MIMO to reduce co-channel interference effects;
- M-MIMO DRA optimization methodology;
- DRA payload optimized architecture for supporting pragmatic M-MIMO.

An alternative to pragmatic M-MIMO is to optimize the design of DRA while exploiting conventional frequency reuse

scheme. For this scenario the following solutions have been developed:

- CFR DRA optimization methodology;
- DRA payload optimized architecture for optimized CFR.

The main findings can be summarized as:

- MB MIQDP-RRM M-MIMO can get close to more complex MF and MMSE solutions with affordable payload complexity and no need for any user feedback apart of the location information.
- For the optimized DRA parameters ZF M-MIMO is under performing the other M-MIMO techniques.
- Optimized DRA design for CFR can get close to pragmatic M-MIMO in terms of performance with even simpler implementation and reduced feeder link bandwidth.

We also have found evidence that by improving the throughput of such a system makes the physical layer to operate in a relative low signal-to-noise plus interference region typically corresponding to QPSK modulation format. In this region the DVB-S2(X) standard is quite sub-optimum compared to Shannon bound and there is a good potential improvement looking at more efficient coding schemes for this "low" spectral efficiency region. This is a recommended research area for the DVB-S2(X) future evolution.

A. EFFICIENT EVALUATION OF ZF AND MMSE PRECODING MATRICES

The evaluation of ZF (27) or MMSE (28) precoding matrices is a computationally expensive operation which depends on the well conditioning of the channel matrix $\mathbf{H}$ and on its size $(N_U \times N_T)$. A dominant element in both (27) and (28) is the inversion of the Gram matrix $\mathbf{H}^H\mathbf{H}$ or its diagonal regularization $\left(\mathbf{H}^H\mathbf{H}+\lambda\mathbf{I}\right)$, respectively. Both matrices have size $(N_T \times N_T)$. Furthermore, considering that for M-MIMO $N_T > N_U$, the Gram matrix $\mathbf{H}^H\mathbf{H}$ is not invertible and use must be done of the Moore-Penrose pseudo inverse [24], [25] which generalize matrix inversion to non-square and ill-conditioned matrices. The uniqueness of the Moore-Penrose pseudo inverse guarantees that whenever either the left pseudo inverse $\left(\mathbf{H}^H\mathbf{H}\right)^{-1}\mathbf{H}^H$, or the right pseudo inverse $\mathbf{H}^H\left(\mathbf{H}\mathbf{H}^H\right)^{-1}$ exists it coincides with the unique Moore-Penrose pseudo inverse of $\mathbf{H}$. At this point it should be noted that while the computational cost of evaluating the two Gram matrices $\mathbf{H}^H\mathbf{H}$ and $\mathbf{H}\mathbf{H}^H$ is the same, the second form exhibits a reduced size $(N_U \times N_U)$ and it is invertible in case the channel matrix $\mathbf{H}$ is full rank. Being the computational cost of matrix inversion roughly proportional to the third power of the size N of the matrix to invert, $\mathcal{O}(N^3)$ the right pseudo inverse offers substantial computational advantage for the evaluation of the zero forcing precoding matrix

$$\mathbf{U}_{\mathrm{ZF}} = \mathbf{H}^H\left(\mathbf{H}\mathbf{H}^H\right)^{-1}. \tag{68}$$

It may now be asked if the MMSE precoder (28) could be obtained in a similarly efficient form as regularization of the right pseudo inverse (68). In the following we demonstrates that this question has a positive answer and that the MMSE precoder can indeed be expressed as

$$\mathbf{U}_{\mathrm{MMSE}} = \mathbf{H}^H\left(\mathbf{H}\mathbf{H}^H+\lambda\mathbf{I}\right)^{-1}, \tag{69}$$

where the regularization constants λ of (28) and (69) are identical.

To prove this result we can start from the form $\mathbf{H}^H\mathbf{H}\mathbf{H}^H + \lambda\mathbf{H}^H$. Factorizing left or right the matrix $\mathbf{H}^H$, we have

$$\begin{aligned}\mathbf{H}^H\mathbf{H}\mathbf{H}^H+\lambda\mathbf{H}^H &= \mathbf{H}^H\left(\mathbf{H}\mathbf{H}^H+\lambda\mathbf{I}\right)\\ &= \left(\mathbf{H}^H\mathbf{H}+\lambda\mathbf{I}\right)\mathbf{H}^H.\end{aligned} \tag{70}$$

The eigenvalues of the the two Gram matrices $\mathbf{H}^H\mathbf{H}$ and $\mathbf{H}\mathbf{H}^H$ coincide and are ≥ 0. If λ is > 0, both $\left(\mathbf{H}\mathbf{H}^H+\lambda\mathbf{I}\right)$ and $\left(\mathbf{H}^H\mathbf{H}+\lambda\mathbf{I}\right)$ are invertible and Eq. (70) can be manipulated multiplying right and left by the two inverses

$$\begin{aligned}&\left(\mathbf{H}^H\mathbf{H}+\lambda\mathbf{I}\right)^{-1}\mathbf{H}^H\left(\mathbf{H}\mathbf{H}^H+\lambda\mathbf{I}\right)\left(\mathbf{H}\mathbf{H}^H+\lambda\mathbf{I}\right)^{-1}\\ &\quad=\left(\mathbf{H}^H\mathbf{H}+\lambda\mathbf{I}\right)^{-1}\left(\mathbf{H}^H\mathbf{H}+\lambda\mathbf{I}\right)\mathbf{H}^H\left(\mathbf{H}\mathbf{H}^H+\lambda\mathbf{I}\right)^{-1},\end{aligned} \tag{71}$$

which can be simplified as

$$\left(\mathbf{H}^H\mathbf{H}+\lambda\mathbf{I}\right)^{-1}\mathbf{H}^H = \mathbf{H}^H\left(\mathbf{H}\mathbf{H}^H+\lambda\mathbf{I}\right)^{-1}. \tag{72}$$

Equation (72) demonstrate the equivalence of (28) with (69) and the superior complexity efficiency of the latter form $\mathcal{O}(N_U^3)$ with respect to the first $\mathcal{O}(N_T^3)$.

B. AGGREGATED CO-CHANNEL INTERFERENCE

Let $\mathbf{Q}$ be a square real positive matrix of size $(N \times N)$ and $\mathbf{C}$ a real positive matrix of size $(N \times C)$, we are interested in the scalar quantity

$$\mathrm{INR}_T = \mathbf{1}^T\left[\mathbf{Q}\odot(\mathbf{C}\mathbf{C}^T)\right]\mathbf{1}, \tag{73}$$

where the $(N \times 1)$ vector $\mathbf{1}$ has all unit entries. Recalling Lemma 7.5.2 in [39]

$$\mathbf{x}^H(\mathbf{A}\odot\mathbf{B})\,\mathbf{y} = \mathrm{tr}\left[\mathrm{diag}(\mathbf{x}^*)\,\mathbf{A}\,\mathrm{diag}(\mathbf{y})\,\mathbf{B}^T\right], \tag{74}$$

substituting $\mathbf{x}=\mathbf{y}=\mathbf{1}$, $\mathbf{A}=\mathbf{Q}$, $\mathbf{B}=\mathbf{C}\mathbf{C}^T$, and noting that $\mathrm{diag}(\mathbf{1})=\mathbf{I}$, and that the product $\mathbf{C}\mathbf{C}^T$ results in a symmetric matrix such that $(\mathbf{C}\mathbf{C}^T)^T = \mathbf{C}\mathbf{C}^T$, we obtain

$$\mathbf{1}^T\left[\mathbf{Q}\odot(\mathbf{C}\mathbf{C}^T)\right]\mathbf{1} = \mathrm{tr}\left(\mathbf{Q}\mathbf{C}\mathbf{C}^T\right). \tag{75}$$

The trace operator is invariant under cyclic permutations, $\mathrm{tr}(\mathbf{ABC}) = \mathrm{tr}(\mathbf{CAB}) = \mathrm{tr}(\mathbf{BCA})$ (refer for example to proof of Eq. 6.299 in [40]), thus we can write

$$\mathrm{tr}\left(\mathbf{Q}\mathbf{C}\mathbf{C}^T\right) = \mathrm{tr}\left(\mathbf{C}^T\mathbf{Q}\mathbf{C}\right). \tag{76}$$

We now make use of the vectorization of a matrix $\mathbf{A}$ of size $(P \times Q)$ into a column vector $\mathrm{vec}(\mathbf{A})$ of size $(PQ \times 1)$ (first

introduced in [41]) obtained by stacking the columns of the matrix A on top of each other

$$\text{vec}(\mathbf{A}) = [a(1,1), \ldots, a(P,1), \ldots, a(1,Q), \ldots, a(P,Q)]^T, \tag{77}$$

and we exploit the compatibility of the vectorization of a matrix with the Frobenius inner product (refer to Eq. 2.11.1 in [41])

$$\text{tr}\,[\mathbf{AB}] = \left[\text{vec}(\mathbf{A}^T)\right]^T \text{vec}(\mathbf{B}), \tag{78}$$

which allows us writing

$$\begin{aligned}\text{tr}\left\{\mathbf{C}^T\mathbf{QC}\right\} &= \left\{\text{vec}[(\mathbf{C}^T\mathbf{Q})^T]\right\}^T \text{vec}(\mathbf{C}) \\ &= \left[\text{vec}(\mathbf{Q}^T\mathbf{C})\right]^T \text{vec}(\mathbf{C}).\end{aligned} \tag{79}$$

Finally, for the compatibility of vectorization with Kronecker product, for the matrices $\mathbf{F}$, $\mathbf{G}$ and $\mathbf{H}$ of sizes $(P \times Q)$, $(Q \times R)$ and $(R \times S)$, respectively, the following identity holds true (refer to Eq. 2.10 in [41])

$$\text{vec}(\mathbf{FGH}) = \left(\mathbf{H}^T \otimes \mathbf{F}\right) \text{vec}(\mathbf{G}). \tag{80}$$

Substituting $\mathbf{F} = \mathbf{Q}^T$, $\mathbf{G} = \mathbf{C}$, and $\mathbf{H} = \mathbf{I}$, we can write

$$\begin{aligned}\left[\text{vec}(\mathbf{Q}^T\mathbf{C})\right]^T &= \left[\left(\mathbf{I}^T \otimes \mathbf{Q}^T\right) \text{vec}(\mathbf{C})\right]^T \\ &= [\text{vec}(\mathbf{C})]^T \left(\mathbf{I}^T \otimes \mathbf{Q}^T\right)^T \\ &= [\text{vec}(\mathbf{C})]^T (\mathbf{I} \otimes \mathbf{Q}),\end{aligned} \tag{81}$$

which provides the final quadratic form

$$\text{INR}_T = \text{tr}\left(\mathbf{C}^T\mathbf{QC}\right) = [\text{vec}(\mathbf{C})]^T (\mathbf{I} \otimes \mathbf{Q}) \text{vec}(\mathbf{C}). \tag{82}$$

REFERENCES

[1] T. L. Mazzetta, "Massive MIMO: An Introduction," *Bell Labs Tech. J.*, vol. 20, pp. 11–20, Mar. 2015.

[2] L. Lu, G. Y. Li, A. L. Swindlehurst, A. Ashikhmin, and R. Zhang, "An overview of massive MIMO: Benefits and challenges," *IEEE J. Sel. Topics Signal Process.*, vol. 8, no. 5, pp. 742–758, Oct. 2014.

[3] G. Caire, L. Cottatelluci, M. Debbah, G. Lechner, and R. Müller, "Interference mitigation techniques for satellite systems," Novel Intra-Syst. Interference Mitigation Techn., Eur. Space Agency, Noordwijk, The Netherlands, Contract No. 18070/04/NL/US Apr. 2005.

[4] L. Cottatellucci, M. Debbah, G. Gallinaro, R. Mueller, M. Neri, and R. Rinaldo, "Interference mitigation techniques for broadband satellite systems," in *Proc. 24th AIAA Int. Commun. Satell. Syst. Conf.*, San Diego, CA, USA, Jun. 2006, p. 5348, doi: 10.2514/6.2006-5348.

[5] D. Christopoulos, S. Chatzinotas, G. Zheng, J. Grotz, and B. Ottersten, "Linear and nonlinear techniques for multibeam joint processing in satellite communications," *EURASIP J. Wireless Commun. Netw.*, vol. 2012, no. 1, p. 162, May 2012.

[6] G. Taricco, "Linear precoding methods for multi-beam broadband satellite systems," in *Proc. 20th Eur. Wireless Conf.*, Barcelona, Spain, May 2014, pp. 1–6.

[7] P.-D. Arapoglou, A. Ginesi, S. Cioni, S. Erl, F. Clazzer, S. Andrenacci, and A. Vanelli-Coralli, "DVB-S2X-enabled precoding for high throughput satellite systems," *Int. J. Satell. Commun. Netw.*, vol. 34, no. 3, pp. 439–455, May 2016.

[8] V. Joroughi, M. Ángel Vázquez, and A. I. Pérez-Neira, "Precoding in multigateway multibeam satellite systems," *IEEE Trans. Wireless Commun.*, vol. 15, no. 7, pp. 4944–4956, Jul. 2016.

[9] *Digital Video Broadcasting (DVB); Second generation framing structure, channel coding and modulation systems for Broadcasting, Interactive Services, News Gathering and other broadband satellite applications; Part 2: DVB-S2 Extensions (DVB-S2X)*, document ETSI EN 302 307-2 V1.1.1, Oct. 2014.

[10] A. Ginesi, E. Re, and P. D. Arapoglou, "Joint beam hopping and precoding in HTS systems," in *Wireless and Satellite Systems* (Lecture Notes of the Institute for Computer Sciences, Social Informatics and Telecommunications Engineering), vol. 231, P. Pillai, K. Sithamparanathan, G. Giambene, M. Vazquez, P. Mitchell, Eds. Cham, Switzerland: Springer, 2017.

[11] B. Devillers, A. Perez-Neira, and C. Mosquera, "Joint linear precoding and beamforming for the forward link of multi-beam broadband satellite systems," in *Proc. IEEE Global Telecommun. Conf.*, Houston, TX, USA., Dec. 2011, pp. 1–6.

[12] L. You, K.-X. Li, J. Wang, X. Gao, X.-G. Xia, and B. Ottersten, "Massive MIMO transmission for LEO satellite communications," *IEEE J. Sel. Areas Commun.*, early access, Jun. 8, 2020, doi: 10.1109/JSAC.2020.3000803.

[13] A. L. Swindlehurst, E. Ayanoglu, P. Heydari, and F. Capolino, "Millimeter-wave massive MIMO: The next wireless revolution?" *IEEE Commun. Mag.*, vol. 52, no. 9, pp. 56–62, Sep. 2014.

[14] E. Björnson, E. G. Larsson, and T. L. Marzetta, "Massive MIMO: Ten myths and one critical question," *IEEE Commun. Mag.*, vol. 54, no. 2, pp. 114–123, Feb. 2016.

[15] R. De Gaudenzi, "Payload nonlinearity impact on the globalstar forward link multiplex. I. physical layer analysis," *IEEE Trans. Veh. Technol.*, vol. 48, no. 3, pp. 960–976, May 1999.

[16] R. L. Cook, "Stochastic sampling in computer graphics," *ACM Trans. Graph.*, vol. 5, no. 1, pp. 51–72, Jan. 1986.

[17] D. M. Sazonov, *Microwave Circuits Antennas*. Chennai, India: MIR, 1990.

[18] Y. Rahmat-Samii, P. Cramer, K. Woo, and S. Lee, "Realizable feed-element patterns for multibeam reflector antenna analysis," *IEEE Trans. Antennas Propag.*, vol. AP-29, no. 6, pp. 961–963, Nov. 1981.

[19] R. Rinaldo and R. De Gaudenzi, "Adaptive coding and modulation for the forward link of satellite broadband multimedia systems," *Int. J. Satell. Commun. Netw.*, vol. 22, no. 3, pp. 401–423, 2004.

[20] P. Angeletti and M. Lisi, "A systemic approach to the compensation of rain attenuation in ka-band communication satellites," *Int. J. Microw. Sci. Technol.*, vol. 2012, pp. 1–7, Oct. 2012, doi: 10.1155/2012/791635.

[21] D. Brennan, "Linear diversity combining techniques," *Proc. IRE*, vol. 47, no. 6, pp. 1075–1102, Jun. 1959.

[22] A. Hessel and J.-C. Sureau, "On the realized gain of arrays," *IEEE Trans. Antennas Propag.*, vol. 19, no. 1, pp. 122–124, Jan. 1971.

[23] T. W. S. Cassels, *An Introduction to Geometry Numbers*. Berlin, Germany: Springer-Verlag, 1959.

[24] E. H. Moore, "On the reciprocal of the general algebraic matrix," *Bull. Amer. Math. Soc.*, vol. 26, no. 9, pp. 394–395, 1920.

[25] R. Penrose, "A generalized inverse for matrices," *Proc. Cambridge Philos. Soc.*, vol. 51, pp. 506–513, May 1955.

[26] C. B. Peel, B. M. Hochwald, and A. L. Swindlehurst, "A vector-perturbation technique for near-capacity multiantenna multiuser Communication—Part I: Channel inversion and regularization," *IEEE Trans. Commun.*, vol. 53, no. 1, pp. 195–202, Jan. 2005.

[27] M. Joham, W. Utschick, and J. A. Nossek, "Linear transmit processing in MIMO communications systems," *IEEE Trans. Signal Process.*, vol. 53, no. 8, pp. 2700–2712, Aug. 2005.

[28] P. Viswanath and D. N. C. Tse, "Sum capacity of the vector Gaussian broadcast channel and uplink–downlink duality," *IEEE Trans. Inf. Theory*, vol. 49, no. 8, pp. 1912–1921, Aug. 2003.

[29] P. Angeletti, "Simple Implementation of Vectorial Modulo Operation based on Fundamental Parallelepiped," *Electron. Lett.*, vol. 48, no. 3, pp. 159–160, Feb. 2012.

[30] P. Angeletti, "Multiple beams from planar arrays," *IEEE Trans. Antennas Propag.*, vol. 62, no. 4, pp. 1750–1761, Apr. 2014.

[31] E. Castaneda, A. Silva, A. Gameiro, and M. Kountouris, "An overview on resource allocation techniques for multi-user MIMO systems," *IEEE Commun. Surveys Tuts.*, vol. 19, no. 1, pp. 239–284, 1st Quart., 2017.

[32] A. Guidotti and A. Vanelli-Coralli, "Geographical scheduling for multicast precoding in multi-beam satellite systems," in *Proc. 9th Adv. Satell. Multimedia Syst. Conf.*, Sep. 2018, pp. 10–12.

[33] P. Angeletti, J. C. Lizarraga Cubillos, "Method and a system of providing multi-beam coverage of a region of interest in multi-beam satellite communication," U.S. Patent 9 654 201, Feb. 27, 2012.

[34] *Satellite Antenna Radiation Pattern for use as a Design Objective in the Fixed-Satellite Service Employing Geostationary Satellites*, document ITU-R S.672-4, 1997.
[35] X. Artiga, M. A. Vázquez, A. I. Perez-Neira, "Large scale multi-antennas over satellites," Eur. Space Agency, Noordwijk, The Netherlands, SatNex IV Tech. Rep., May 2019.
[36] M. Miller, "Capacity maximization for a unicast spot beam satellites system," U.S. Patent 8 010 043, Jul. 20, 2007.
[37] R. De Gaudenzi, N. Alagha, M. Angelone, and G. Gallinaro, "Exploiting code division multiplexing with decentralized multiuser detection in the satellite multibeam forward link," *Int. J. Satell. Commun. Netw.*, vol. 36, no. 3, pp. 239–276, May 2018, doi: 10.1002/sat.1215.
[38] C. Topping, A. Bishop, T. Craig, D. Howe, J. Hamer, P. Angeletti, and A. Senior, "S-UMTS processor key technologies demonstrator," in *Proc. 10th Int. Workshop Signal Process. Space Commun.*, Rhodes Island, Greece, Oct. 2008, pp. 6–8.
[39] R. A. Horn, C. R. Johnson, *Matrix Analysis*, 2nd ed. Cambridge, U.K.: Cambridge Univ. Press, 2012.
[40] C. D. Cantrell, *Modern Mathematical Methods for Physicists Engineers*. Cambridge, U.K.: Cambridge Univ. Press, 2000.
[41] H. Neudecker, "Some theorems on matrix differentiation with special reference to Kronecker matrix," *J. Amer. Stat. Assoc.*, vol. 64, pp. 953–963, 1969.
[42] P. Angeletti, "Reconfigurable beam-forming-network architecture," U.S. Patent 8 451 172, Sep. 10, 2010.

PIERO ANGELETTI (Senior Member, IEEE) received the Laurea degree *(summa cum laude)* in electronics engineering from the University of Ancona, Italy, in 1996, and the Ph.D. degree in electromagnetism from the University of Rome La Sapienza, Italy, in 2010. He has more than 20 years of experience in RF systems engineering and technical management encompassing conceptual/architectural design, trade-offs, detailed design, production, integration and testing of satellite payloads, and active antenna systems for commercial/military telecommunications and navigation (spanning all the operating bands and set of applications) as well as for multifunction RADARs and electronic counter measure systems. He is currently a Member of the Technical Staff of the European Space Research and Technology Center (ESTEC), European Space Agency, Noordwijk, The Netherlands. He is heading the Radio Frequency Payloads and Technology Division, Directorate of Technology, Engineering and Quality (TEC), which is responsible for RF payloads, instruments, and relevant technologies. In particular, he oversees ESA research and development activities related to flexible satellite payloads, RF front-ends, and on-board digital processors. He has authored/coauthored over 300 technical reports, book chapters, and articles published in peer reviewed professional journals and international conferences' proceedings. He holds several patents related to satellite payload and antenna technology. Together with Giovanni Toso, he is an Instructor of the course on Multibeam Antennas and Beamforming Networks, which has been offered at main IEEE and European microwaves, wireless and antenna conferences (the IEEE APS, the IEEE IMS, EuMW, EuCAP, the IEEE ICWITS, ESA Internal University, and so on), since 2012.

RICCARDO DE GAUDENZI (Senior Member, IEEE) received the Dr. Eng. degree *(cum laude)* in electronic engineering from the University of Pisa, Italy, in 1985, and the Ph.D. degree from the Delft University of Technology, The Netherlands, in 1999. From 1986 to 1988, he was with the European Space Agency (ESA), Stations and Communications Engineering Department, Darmstadt, Germany, where he was involved in satellite telemetry, tracking, and control (TT&C) ground systems design and testing. In 1988, he joined the ESA's Research and Technology Centre (ESTEC), Noordwijk, The Netherlands, where he has been covering several technical and managerial positions inside the Directorate of Technology, Engineering and Quality. He is currently the Head of the ESA's Electrical Engineering Department. The department covers radio-frequency systems and payloads for navigation, telecommunication TT&C and earth observation, EEE components and microelectronics, data handling systems, power systems and energy sources, electromagnetic compatibility, and space environments and their effects. He has been responsible for a large number of research and development activities for TT&C, telecom, and navigation applications. In 1996, he spent one year with Qualcomm Inc., San Diego, CA, USA, in the Globalstar LEO Project System Group under the ESA Fellowship. His current interest is mainly related with efficient digital modulation and multiple access techniques for fixed and mobile satellite services, synchronization topics, adaptive interference mitigation techniques, and communication systems simulation techniques. He actively contributed to the development and the demonstration of the ETSI S-UMTS Family A, S-MIM, DVB-S2, DVB-S2X, DVB-RCS2, and DVB-SH Standards. He has published more than 140 scientific articles and own more than 28 patents. He was a co-recipient of the 2003 and 2008 Jack Neubauer Memorial Award Best Paper from the IEEE Vehicular Technology Society. From 2001 to 2005, he has served as an Associate Editor for CDMA and Synchronization for the IEEE TRANSACTIONS ON COMMUNICATIONS and an Associate Editor for the *Journal of Communications and Networks*.